Ecosystem Heterogeneity Determines the Ecological Resilience of the Amazon to Climate Change
SUPPORTING INFORMATION APPENDIX

Naomi M. Levine[1,2]
Ke Zhang[1, 3]
Marcos Longo[4,5]
Alessandro Baccini[6]
Oliver L. Phillips[7]
Simon L. Lewis[7,8]
Esteban Alvarez-Dávila[9]
Ana Cristina Segalin de Andrade[10]
Roel Brienen[7]
Terry Erwin[11]
Ted R. Feldpausch[12]
Abel Lorenzo Monteagudo Mendoza[13]
Percy Nuñez Vargas[14]
Adriana Prieto[15]
Javier Eduardo Silva Espejo[14]
Yadvinder Malhi[16]
Paul R. Moorcroft[1]

[1] Department of Organismic and Evolutionary Biology, Harvard University, Cambridge, MA
[2] Department of Biological Sciences, University of Southern California, Los Angeles, CA
[3] Cooperative Institute for Mesoscale Meteorological Studies, University of Oklahoma, Norman, OK
[3] Department of Earth and Planetary Sciences, Harvard University, Cambridge, MA
[4] Embrapa Satellite Monitoring, Campinas, SP, Brazil
[5] The Woods Hole Research Center, 149 Woods Hole Road, Falmouth, MA
[6] School of Geography, University of Leeds, Leeds, UK
[7] Department of Geography, University College London, London, UK
[8] Jardín Botánico de Medellín, Grupo de Investigación en Servicios Ecosistémicos y Cambio Climático, Medellín, Colombia.
[9] Instituto Nacional de Pesquisas da Amazônia, Manaus, Brazil
[10] Department of Entomology, Smithsonian Institution, Washington DC
[11] College of Life and Environmental Sciences, University of Exeter, Exeter, UK
[12] Jardín Botánico de Missouri, Oxapampa, Perú
[13] Universidad Nacional de San Antonio Abad del Cusco, Cusco, Perú
[14] Instituto de Ciencias Naturales, Bogotá, Colombia
[14] School of Geography and the Environment, University of Oxford, Oxford, UK

Corresponding author: *Paul R. Moorcroft*
26 Oxford St., Cambridge, MA 02138, USA
paul_moorcroft@harvard.edu, (617) 496-6744

SI Appendix S1: Analysis of the Spatial Pattern Above-Ground Biomass and the Impacts of Anthropogenic Activity and Fire

Regional Analysis: The distribution of above-ground biomass across the Amazon basin was evaluated using two independent satellite products, *Baccini et al. (1)* and *Saatchi et al. (2)*. Although these two estimates vary on a point-by-point basis by up to 80%, they are also significantly correlated with each other (r^2=0.75 p<0.01). Both satellite-based estimates show a similar overall distribution of above-ground biomass (AGB) across the basin, with a continual and gradual transition from high biomass forests to low biomass savannah (*Fig. 1b main text*). Dry season length (DSL) explains approximately half of the variance in the satellite-based estimates of AGB with a Spearman correlation coefficient of -0.75 for the *Baccini* dataset (r^2=0.56, p<0.01), and -0.59 for the *Saatchi* dataset (r^2=0.35, p<0.01) (*Fig. 1 main text*). Across the RAINFOR plot-based measurements (*n*=59, *Table S1*), AGB also decreases as DSL increases (*Fig. 1, main text*); however, the relationship is not statistically significant (p=0.31, *n*=59).

Deforestation contributes significantly to AGB spatial heterogeneity in the Amazon region; however, in this study, we focus on the impacts of climate change on Amazonian forests. To this end, all model simulations were conducted without anthropogenic disturbance (i.e. logging, slash-and-burn activities, or any other human-derived deforestation). To minimize the impact of anthropogenic activities on the remote-sensing AGB datasets, we first filtered the data using the European Space Agency GlobCover data (4) (300 m resolution) to remove all pixels with greater than 5% degraded or disturbed forests or open water. We used the GlobCover dataset as it provides the best-available spatial coverage of the basin. The resulting primary vegetation dataset (≥ 95% intact forest) was then aggregated (as mean AGB per m^2 ground) to 1° x 1° for comparison against the model simulations, which were run at 1° due to the resolution of the Sheffield *et al.* (5) climate dataset, the best-available climatology for the region. Spatial

heterogeneity in biomass with dry season length was calculated for two different spatial scales: high-resolution (500 m for *Baccini et al.,* 1 km for *Saatchi et al.*), and course-resolution (1° aggregates). Specifically,

$$AGB\ variability_i = {}^{\sigma_j}/_{\mu_j}\,, \qquad (S1)$$

where *j* represents all pixels with dry season length equal to *i*. In order to remove grasslands from the analysis, only pixels with greater than 2 kg C m^{-2} of above-ground biomass were included. This low threshold value was chosen in order to include dry forest regions and the transition to savannah-like cerrado ecosystems. The change in spatial heterogeneity with dry season length for the high-resolution dataset was calculated by downscaling the 1° Sheffield *et al.* climatology (5) using bi-linear interpolation in order to create a dry season length map with 500 m and 1 km resolution. The results of the AGB variability analysis are shown in *Figure 1* (*main text*) and *Figure S1b*. We have also repeated the analysis using the higher spatial resolution, but lower spatial coverage, Brazilian National Institute For Space Research (INPE) PRODES (Programa de Cálculo do Desflorestamento da Amazônia) data (6) (90 m resolution). The change in spatial heterogeneity with dry season length was evaluated both as a percentage change relative to mean AGB, coefficient of variation (1σ/mean, equation 1), and as an absolute value (1σ).

Both satellite-based estimates show the same relationship of increasing site-to-site variability in AGB with increasing DSL (*Fig. 1c main text, and Fig. S1b*), with a correlation between the coefficients of variation for the two high-resolution datasets of r^2=0.97 ($p<0.01$). The same trend is also observed when plotted as an absolute value. The trend seen in the remote-sensing datasets is consistent with the statistically significant increase in spatial heterogeneity with increasing DSL seen in the RAINFOR plots (*Fig. 1 main text, and Fig. S1b*), where recent, detectable anthropogenic activity is absent.

Effects of fire: Fire is known to be an important factor in the genesis of spatial heterogeneity in AGB. However, there is no evidence of recent fire disturbance in the RAINFOR plots suggesting that the significant increase in biomass spatial heterogeneity with increasing DSL is driven by an additional mechanism. This conclusion is reinforced by the statistically significant increase in spatial heterogeneity in the remote-sensing datasets for dry seasons of less than 3 months (*Fig. 1, $p < 0.01$*) where fire activity is generally low (7).

While fire and water stress both reduce forest biomass, these two processes have different impacts on forest composition and function. Recent field studies show that fires, specifically understory fires, do not have a significant impact on carbon cycling (net primary production (NPP) and respiration) relative to control plots (8), but do result in lower stem densities due to increased seedling and understory mortality (9, 10). This contrasts with significant decreases in above-ground NPP and increased mortality of canopy trees relative to control plots seen during the Tapajos throughfall exclusion experiments (11, 12). Therefore, accurately representing both processes in ecosystem models is essential in order to capture forest dynamics in response to perturbations. While fire will accelerate the transition from low biomass forests to savannah (10), we expect that, in the absence of fire, moist tropical forests will nonetheless transition to lower biomass tropical forests as a result of climate-induced increases in the magnitude of plant-level water stress.

The impact of fires on the Amazonian response to changes in climate were recently analyzed by *Zhang et al. (13)* who conducted a series of regional simulations with the ED2 model forced with increasing CO_2 and observed and projected climate from 1715 – 2100 under the SRES A2. As seen in *Figure S2*, fires act to increase the fraction of the basin with low biomass. However, while this creates a more bi-modal distribution in biomass, in both the

present day and 2100, the region's ecosystems still show a gradual transition from high biomass moist tropical forests through dry forests and savannah-like biomes to grasslands.

Table S1: RAINFOR data used for model-observation comparison. Data are from Baker et al. 2004a, Baker et al. 2004b, Phillips et al. 2004, Sheffield et al. 2006, and Quesada et al. 2010. AGB and wood density values are from the year identified in the table. Mortality rates are calculated over the census interval which is given in Phillips et al. 2004.

Site Name	**Lat**	**Lon**	**Year**	**Sand fraction** Quesada et al. (18)	**Clay fraction** Quesada et al. (18)	**DSL (month)** Sheffield et al. (5)	**AGB** **in kg C m^{-2}** Baker et al (3)	**Wood Density** **in g cm^{-3}** Baker et al. (34)	**Mortality** **in % yr^{-1}** Phillips et al. (33)
ALP-11	-3.95	-73.43	2001	0.53	0.21	0.44	13.48	0.60	3.24
ALP-12	-3.95	-73.43	2001	0.78	0.10	0.44	13.32	0.63	2.94
ALP-21	-3.95	-73.43	2001	0.94	0.03	0.44	14.38	0.62	2.47
ALP-22	-3.95	-73.43	2001	0.33	0.34	0.44	12.05	0.54	2.32
BDF-01	-2.4	-60	1999	N/A	N/A	2.79	18.93	0.72	1.44
BDF-03	-2.4	-59.9	1999	N/A	N/A	3.54	16.95	0.66	1.53
BDF-04	-2.4	-59.9	1999	N/A	N/A	3.54	12.53	0.67	3.54
BDF-05	-2.4	-59.9	1999	N/A	N/A	3.54	15.21	0.69	2.32
BDF-06	-2.4	-59.9	1999	N/A	N/A	3.54	14.75	0.68	1.87
BDF-08	-2.4	-59.9	1999	N/A	N/A	3.54	15.95	0.66	--
BDF-10	-2.4	-59.9	1997	N/A	N/A	3.54	16.34	0.67	1.73
BDF-11	-2.4	-59.9	1997	N/A	N/A	3.54	17.74	0.69	0.84
BDF-12	-2.4	-59.9	1997	N/A	N/A	3.54	17.45	0.69	0.75
BDF-13	-2.4	-60	1998	N/A	N/A	2.79	17.11	0.70	1.20
BDF-14	-2.4	-60	1998	N/A	N/A	2.79	17.81	0.68	1.59
BNT-01	-2.38	-60.1	1999	N/A	N/A	2.79	18.52	--	1.12
BNT-02	-2.38	-60.1	1999	N/A	N/A	2.79	19.48	--	0.78
BNT-04	-2.38	-60.1	1999	0.16	0.68	2.79	16.60	--	1.50
BNT-05	-2.38	-60.1	1993	N/A	N/A	2.79	16.20	--	1.78
BNT-06	-2.38	-60.1	1993	N/A	N/A	2.79	18.18	--	1.67
BNT-07	-2.38	-60.1	1993	N/A	N/A	2.79	17.93	--	1.18
BOG-01	-0.7	-76.48	2002	0.36	0.29	0.46	14.47	0.54	2.40
BOG-02	-0.7	-76.47	2002	0.47	0.30	0.46	11.10	0.53	3.41
CAX-01	-1.7	-51.53	2002	0.64	0.25	3.72	18.94	0.71	1.06
CAX-02	-1.7	-51.53	2003	0.24	0.46	3.72	18.23	0.68	1.46
CHO-01	-14.35	-61.16	2001	0.58	0.36	5.97	6.24	0.56	2.96
CRP-01	-14.54	-61.48	2001	0.63	0.18	5.97	10.68	0.65	2.69

Table S1 cont

Site Name	**Lat**	**Lon**	**Year**	**Sand fraction** Quesada et al. (18)	**Clay fraction** Quesada et al. (18)	**DSL (month)** Sheffield et al. (5)	**AGB** **in kg C m^{-2}** Baker et al (3)	**Wood Density** **in g cm^{-3}** Baker et al. (34)	**Mortality** **in % yr^{-1}** Phillips et al. (33)
CRP-02	-14.53	-61.48	2001	0.84	0.07	5.97	11.69	0.55	--
CUZ-01	-12.5	-68.95	1998	N/A	N/A	4.28	14.17	0.59	2.03
CUZ-02	-12.5	-68.95	1998	N/A	N/A	4.28	12.43	0.53	1.81
CUZ-03	-12.49	-69.11	1998	0.05	0.42	2.87	12.51	0.58	2.55
CUZ-04	-12.49	-69.11	1998	N/A	N/A	2.87	14.46	0.57	2.55
HCC-21	-14.56	-60.75	2001	0.22	0.40	5.90	12.46	0.58	3.24
HCC-22	-14.57	-60.74	2001	0.66	0.21	5.90	13.54	0.59	2.03
JAC-01	-2.38	-60.1	2002	N/A	N/A	2.79	15.79	--	1.19
JAC-02	-2.38	-60.1	2002	N/A	N/A	2.79	15.58	--	1.28
JAS-02	-1.07	-77.6	2002	0.41	0.29	0.64	12.40	0.49	2.45
JAS-03	-1.07	-77.67	2002	0.40	0.33	0.64	13.14	0.50	2.36
JAS-04	-1.07	-77.67	2002	0.42	0.31	0.64	15.93	0.51	1.43
JAS-05	-1.07	-77.67	2002	0.35	0.32	0.64	14.34	0.49	2.57
JRI-01	-1	-52.05	1996	0.04	0.81	4.00	19.35	0.71	1.41
LFB-01	-14.61	-60.87	2001	0.74	0.20	5.90	12.00	0.58	3.22
LFB-02	-14.6	-60.85	2001	0.73	0.21	5.90	14.25	0.57	--
LSL-01	-14.4	-61.13	2001	0.29	0.36	5.97	8.67	0.60	3.25
LSL-02	-14.4	-61.13	2001	0.29	0.36	5.97	10.18	0.55	1.35
SUC-01	-3.23	-72.9	2001	0.38	0.47	0.77	13.93	0.58	2.41
SUC-02	-3.23	-72.9	2001	0.32	0.46	0.77	14.37	0.60	3.01
TAM-01	-12.85	-69.28	2000	0.18	0.29	2.87	13.00	0.53	2.73
TAM-02	-12.83	-69.28	2000	0.20	0.40	2.87	13.00	0.54	1.91
TAM-04	-12.83	-69.28	1998	0.17	0.39	2.87	14.43	0.60	3.00
TAM-05	-12.83	-69.28	2000	0.40	0.44	2.87	13.31	0.60	2.92
TAM-06	-12.83	-69.3	2000	0.02	0.46	2.87	14.10	0.51	1.93
TAM-07	-12.83	-69.27	1998	0.47	0.29	2.87	12.86	0.56	3.17
TAP-01	-3.31	-54.94	1995	0.23	0.66	4.21	14.81	0.65	0.84
TAP-02	-3.31	-54.94	1995	0.23	0.66	4.21	18.69	0.69	0.74
TAP-03	-3.31	-54.94	1995	0.23	0.66	4.21	18.86	0.67	1.00
TIP-02	-0.63	-76.14	2002	N/A	N/A	0.46	13.04	0.57	2.30
TIP-03	-0.64	-76.15	2002	0.03	0.57	0.46	12.76	0.60	2.85
YAN-01	-3.43	-72.85	2001	0.32	0.27	0.77	14.96	0.53	3.11

SI Appendix S2: Analysis of the Impacts of Soil Texture and Fertility on Regional Patterns of Above-ground Biomass

Soil texture, physics, and fertility have been shown to correlate with forest structure, function, and composition (14-16). *Quesada et al.* (15) find that forest growth rates are significantly correlated with soil phosphorus content; forest turnover and wood density are correlated with soil physics; and above-ground biomass is best predicted using phosphorus, potassium, dry season precipitation, and soil physics. The *Quesada et al.* study provides an analysis of basin wide patterns that differs from patterns observed at finer scales, such as those seen by *Laurance et al.* (17) who found no relationship between AGB and phosphorus, but a strong positive correlation between soil clay content, soil nitrogen, and AGB. We investigate the impact soils may have in driving the observed increase in biomass spatial heterogeneity with increasing dry season length using the datasets of *Quesada et al.* (18). Here we use total extractable phosphorus as a proxy for soil fertility based on the analysis of *Quesada et al.* (15), which indicates that this quantity was most significantly correlated with above-ground biomass across the basin. We find no statistically significant change in the mean or variance of the total extractable phosphorus with increasing dry season length from 0 to 6 months (*Fig. S3, Table S2*).

The analysis was repeated with soil clay fraction using both the dataset of *Quesada et al.* (18) and a hybrid regional dataset combining IGBP-DIS(19) and Quesada *et al.* soil data (*see SI Appendix S3 for further detail on the hybrid soil dataset*). The Quesada *et al.* dataset showed no significant change in the mean or variance in soil clay fraction with increasing dry season length from 0 to 6 months (*Fig. S3, Table S2*). The hybrid regional dataset shows no significant change in the variance in soil clay fraction, but exhibits a small, statistically-significant increase in mean clay content with increasing dry season length (*Fig. S3, Table S2*). The increase in mean clay

fraction is relatively small (0.10 over a 6 month change in dry season length, r^2=0.08 p <0.01), especially relative to the 50% increase in above-ground biomass spatial variability. This correlated trend in mean soil clay content may accentuate the response to changes in dry season length as demonstrated by the suite of ensemble model simulations (see *SI Appendix S5*); however, it is difficult to attribute a change in above-ground biomass (AGB) spatial heterogeneity to a change in mean soil texture alone. One would anticipate that the change in AGB spatial heterogeneity would be driven by a change in the variability of soil texture, which was not observed in either the hybrid dataset or the Quesada *et al.* dataset. There was also no trend in the soil clay fraction coefficients of variation with dry season length for either dataset (*Table S2*).

While this analysis suggests that basin-wide gradients in soil type are not the dominant mechanism influencing the large-scale pattern of spatial variation in above-ground biomass across the Amazon, as is shown in the main text, soil texture heterogeneity becomes increasingly important in influencing AGB as dry season length increases and climate transitional points are reached (*Fig. 2 main text)*. In this analysis we have focused on dry season length and its impacts on soil moisture availability; however, differences in soil nutrient availability at both regional and local scales, and the interaction between soil fertility, soil texture, and dry season length, will also influence patterns of Amazonian AGB. At the basin-scale, forests on the younger, more fertile soils of western Amazonia have higher rates of biomass productivity, but lower AGB than the forests of the central Amazon and Guianan Shield, that are located on older, nutrient-poor soils, with this difference being accounted for by correlated changes in stem turnover (15, 20). At the landscape-scale, differences in nutrient availability have been identified as an important factor accounting for the lower AGB found in Amazon white sand forests compared to the higher

AGB found on neighboring clay soils that have higher nutrient availability (e.g. 17, 21). Incorporating and validating nutrient dynamics in terrestrial ecosystem models is an important, ongoing avenue of research that will ultimately allow us to address these important and complex interactions.

Table S2: Mean and 1σ standard deviation of total extractable phosphorus and clay fraction as a function of dry season length. The coefficients of variation (σ/μ) are given in parentheses.

Dry Season Length (month)	Total Extractable Phosphorus (mg kg^{-1})		Clay fraction (*Quesada et al.*)		Clay fraction (*hybrid*)	
0-1	278.7 ± 221.5 (79%)	N=25	0.28 ± 0.14 (50%)	N=25	0.27 ± 0.06 (21%)	N=90
1-2	28.5 ± 4.1 (14%)	N=2	0.10 ± 0.14 (133%)	N=2	0.28 ± 0.09 (33%)	N=58
2-3	263.7 ± 215.8 (82%)	N=12	0.44 ± 0.24 (54%)	N=13	0.30 ± 0.09 (29%)	N=101
3-4	195.2 ± 92.2 (47%)	N=5	0.35 ± 0.13 (38%)	N=6	0.33 ± 0.09 (27%)	N=162
4-5	146.4 ± 80.6 (55%)	N=11	0.40 ± 0.30 (75%)	N=12	0.36 ± 0.10 (28%)	N=195
5-6	375.4 ± 231.1 (62%)	N=10	0.24 ± 0.12 (48%)	N=10	0.34 ± 0.11 (31%)	N=206

SI Appendix S3: Description of ED2 and ED2-BL Model Formulations and Model Simulations

ED2 formulation: A detailed description of the Ecosystem Demography Model (ED2) used in this study can be found in *Moorcroft et al. (22)* and *Medvigy et al. (23)*. As a size-and-age structured terrestrial ecosystem model, ED2 represents the dynamics of individual plants within a horizontally and vertically heterogeneous canopy. The underlying biochemical, physiological, and biomechanical traits of individuals (e.g. maximum photosynthetic capacity, leaf life span, specific leaf area, wood density, and density independent morality) are determined by an individual's plant functional type (*Table S3a*) and do not vary as a function of size of the individual. However, as individuals grow in diameter and height according to the allometric relationships in *Table S3b*, their size influences access to light within the canopy and water in the soil. Consequently, growth and mortality rates of individuals are influenced by plant size and the horizontal and vertical heterogeneity of the canopy. In particular, smaller trees have shallower rooting depths (defined as a function of plant height), and consequently only have access to water in shallow soil layers, while taller trees have deep rooting depths and consequently access both shallow and deep soil layers. Similarly, small trees are shaded by taller ones and thus have limited access to light. The canopy aggregated carbon pools and growth and mortality rates of the forest are therefore a function of both the composition and the size structure of the forest. The impacts of individual-based dynamics on drought sensitivity are discussed in further detail in *SI Appendix S6*.

The model parameterization used in this analysis closely follows the parameterization developed for tropical forests by *Moorcroft et al. (22),* with four relatively minor adjustments. First, the drought deciduous phenology of tropical tree plant functional types (PFTs) was modified slightly from the original formulation in *Moorcroft et al.(22)* so that trees gradually

shed their leaves once available soil water falls below a prescribed water stress threshold (θ_{crit}), rather than the instantaneous, step-wise nature of leaf drop in the original ED model formulation. This change reflects the fact the ED2 terrestrial model solves for the fast-timescale fluxes of carbon, water and energy in the plant canopy. In addition, the critical water threshold (θ_{crit}=0.11) was changed to be defined as the ratio of available soil water relative to the maximum potential available water, where θ_{crit} is the depth averaged θ_{dz} where:

$$\theta_{dz} = \big(\theta(z) - \theta_{wp}\big)/\big(\theta_s - \theta_{wp}\big),$$

and $\theta(z)$ is the ten-day average of the instantaneous volumetric soil moisture content, θ_{wp} is the volumetric soil moisture content at the wilting point (see definition below), and θ_s is the volumetric soil moisture content at saturation. In order to maintain the same threshold for leaf drop as in the original formulation, θ_{crit} was rescaled. As θ_s and θ_{wp} vary by soil texture, the rescaling calculated was made using sandy loam soil (e.g. Manaus site, MAN-04) as this was one of the sites used in the original *Moorcroft et al.*(22) manuscript. The consistency of this revised θ_{crit} with the older version was confirmed using Jaru (RJA), Santarem KM67, the through-fall exclusion site at Caxiuana, and Rio Branco as test sites. Because the new formulation results in gradual leaf drop after the threshold has been reached, the model is not acutely sensitive to the choice of threshold value.

Second, soil properties were calculated from sand (*xsand)* and clay (*xclay)* fractions following *Cosby et al.* (24) where:

$$b = 3.10 + 15.7xclay - 0.3xsand,$$
$$\psi_s = (10^{2.17-0.63xclay-1.58xsand}) * 0.01,$$
$$\mathrm{K}_s = (10^{-0.60-0.64xclay+1.26xsand}) * \left(\frac{0.0254}{3600}\right),$$
$$\theta_s = \frac{50.5-3.7xclay-14.2xsand}{100},$$

and where:

b = constant,

Ψ_s = moisture potential (soil matrix suction) at saturation (m),

K_s = hydraulic conductivity at saturation (m/s),
θ_s = volumetric soil moisture content at saturation (m^3/m^3) (*Fig. S4a*),

and (*Clapp and Hornberger* (25) equations 1 and 2):

$$\psi = \psi_s \left(\frac{\theta_s}{\theta}\right)^b,$$
$$K = K_s \left(\frac{\theta}{\theta_s}\right)^{2b+3}.$$

From the above equations, the volumetric soil moisture at the critical point/field capacity (θ_{fc}), wilting point (θ_{wp}), and air dry point (θ_{ad} (in m^3/m^3) were calculated where:

- The *field capacity* or *critical point* was defined as a hydraulic conductivity of 0.1 mm/day (or K_{fc}=1.157e-9 m/s).
- The *wilting point* was defined as a matrix potential of -1.5MPa or equivalently Ψ_{wp}=1500/g where g is the gravitational constant
- The *air dry point* was defined as a matrix potential of -3.1MPa or equivalently Ψ_{ad}=3100/g where g is the gravitational constant

Such that:

$$\theta_{fc} = \theta_s \left(\frac{K_{fc}}{K_s}\right)^{1/2b+3},$$
$$\theta_{wp} = \theta_s \left(\frac{\psi_s}{\psi_{wp}}\right)^{1/b},$$
$$\theta_{ad} = \theta_s \left(\frac{\psi_s}{\psi_{ad}}\right)^{1/b}.$$

θ_{fc} and θ_{wp} as a function soil texture are shown in panels b and c of *Figure S4* respectively.

Third, the photosynthetic parameters (maximum photosynthetic capacity and dark respiration) of the plant functional types were adjusted using site-level measurements of Gross Primary Productivity (GPP), Net Ecosystem Productivity (NEP), and above-ground biomass (AGB) from the Manaus KM34 flux tower site. Other than this adjustment that used data from a single plot location, the model was not tuned, fitted, or optimized against RAINFOR

measurements. Finally, fire dynamics were not allowed to occur in any of the simulations conducted in this analysis.

In contrast to conventional terrestrial biosphere models in which mortality is represented implicitly as part of the overall rate of tissue turnover, ED2 explicitly models the dynamics of individual mortality. Following Moorcroft *et al. (22),* the probability of mortality per unit time for an individual stem (i) within the canopy is governed by the sum of three terms:

$$mort_i(t) = \mu_{PFT_i} + \mu_{CB_i}(t) + \lambda(t),$$

a mortality term reflecting the differential longevity of different plant functional types (μ_{PFT}) ; a mortality term governed by an individual's rate of carbon accumulation ($\mu_{CB}(t)$); and a third term reflecting mortality arising from stochastic disturbance events $\lambda(t)$.

Specifically, the density-independent term (μ_{PFT}) increases as a linear function of the wood density of the plant functional type (ρ_{PFT}, Table 3a):

$$\mu_{PFT_i} = m_1\left(1 - {\rho_{PFT}}/{\rho_{LS}}\right),$$

where ρ_{LS} is the wood density of the late-successional plant functional type, and the parameter $m_1 = 0.15$. The carbon balance mortality term $\mu_{CB}(t)$ is given by:

$$\mu_{CB_i}(t) = \frac{m_2}{\left(1+e^{m_3\frac{CB_i(t)}{CB_{FS_i}}}\right)},$$

where m_2 and m_3 are constants set to 10 and 20, respectively, $CB_i(t)$ is the net carbon balance of the individual, defined as its gross primary production (kg C m^{-2} yr^{-1}) minus its respiration and tissue maintenance costs, and CB_{FSi} (kg C m^{-2} yr^{-1}) is the plant's net carbon balance in full sunlight. For the simulations presented in this analysis, mean $\mu_{CB}(t)$ for the canopy typically ranged from 0 to 0.012 y^{-1}.

In the absence of fire, the rate of disturbance ($\lambda(t)$) was 0.014 y^{-1}, representing a fixed background rate of canopy gap formation. Survivorship for understory trees (<10m) during gap formation is 10% (i.e. conditional on a canopy tree-fall disturbance event occurring, the mortality for understory trees is 90%). The above function gives longevities consistent with empirical estimates, ranging from 13 years for the early successional tree type to 71 years for the late-successional tree type.

ED2-BL formulation: To evaluate the role of individual competition in the model dynamics, we created ED2-BL, a horizontally- and vertically-averaged analog of the ED2 model. In the native ED2 model formulation, the plant canopy is represented as a vertically-structured and horizontally heterogeneous mixture of individuals of different plant functional types that compete locally for light and water (*described above*). ED2-BL represents exactly the same biophysical and biogeochemical processes as ED2; however, the size- and age-structured canopy is replaced with a horizontally- and vertically- averaged canopy akin to those used by conventional terrestrial biosphere models (e.g. 26). Specifically, instead of a spatially heterogeneous vertical canopy composed of individuals of different species and size (height) competing directly for resources (water and light), in ED2-BL the plant functional types occupy distinct fractions within each grid cell. The canopy within each fractional area is represented as a single-height canopy at 35 m for tropical trees and 1.5 m for tropical grasses, as is standard for many conventional terrestrial biosphere models. In ED2, individuals start as seedlings (0.5 m height) and grow to canopy trees (35m height). Once they pass a minimum reproductive height (5 m), individuals in ED2 allocate a fraction of their excess carbon into seed biomass, which is then transformed into 0.5 m seedlings with a population proportional to the total carbon available

after accounting for seedling mortality. In ED2-BL, all individual trees have a height of 35 m and excess carbon is used to increase the number of individual trees of a given PFT, and the accompanying canopy-level leaf area index (LAI) for the PFT. In ED2-BL, the individual-based allometry of ED2 is replaced with a single aggregated canopy allometry in which the ratio of foliar biomass to stem biomass was adjusted to be consistent with observed canopy-scale relationships between these two quantities. *Table S3(a,b)* provides a list of the physiological, allometric, and life history parameters of the different plant function types used in ED2 and ED2-BL.

Similar to other aggregated, 'ecosystem-as-big-leaf" terrestrial biosphere models (e.g. 27), the different PFTs in ED2-BL compete against each other by expanding their fractional area within the grid-cell. The fractional area occupied by each functional type (i) in ED2-BL is determined as:

$$A_i = {}^{LAI_i}/_{LAI_{total}},$$

where LAI_{total} is the LAI summed over all PFTs.

Regional Simulations: ED2 and ED2-BL model simulations were conducted for the entire Amazon basin at 1° x 1° resolution, due to climatological driver resolution. A regional soil map at 1° x 1° resolution was generated from the observation-based soil maps of *Quesada et al.* (18) and the IGBP-DIS soil map (19). Specifically, the Quesada data (1 km resolution, single depth) was converted from soil type to sand and clay fraction using the mean sand and clay fraction of each soil class. This dataset covered 71% of the region. Remaining pixels were filled in with the IGBP-DIS data (0.5° resolution, upper 4 m) using depth averaged soil and clay fractions. A 1° resolution soil map was then generated from the 1 km map using the arithmetic mean for each 1°

grid cell. Following *Zhang et al*. (13), a soil depth of 10 m with a free bottom boundary was used for the regional simulations. In addition, ED2 was run for nine intensively-studied RAINFOR sites using soil depth and the bottom boundary condition of the soil column specified from site-specific measurements (*Table S4*), and for 37 RAINFOR sites for which soil texture and AGB estimates were available (*Table S1*). The simulations were forced with 39 years (1970-2008) of downscaled reanalysis-derived data (5). The meteorological drivers consisted of atmospheric temperature (3-hourly), specific humidity (6-hourly), shortwave radiation (45 minute), longwave radiation (3-hourly), precipitation (hourly), wind-speed (6-hourly), and pressure (3-hourly). Shortwave (SW) radiation was divided into visible and near-infrared, and further into direct and diffuse radiation following *Goudriaan* (28). All simulations were started from a near-bare-ground ecosystem state and run to equilibrium under pre-industrial atmospheric CO_2 (278ppm) by cycling over the driver data. Equilibrium was defined as less than a 0.7% change per year in AGB over a 30-year period. Most simulations had less than a 0.01% change in AGB per year after 500 years. From the equilibrium state, the simulations were then continued from 1715-2008 forced with increasing atmospheric CO_2 based on ice-core data and the IPCC estimates (29). The results of these simulations are shown in *Figure 1* and *Figure S1*.

Ensemble model simulations with varying soil texture: Four sets of ensemble model runs were conducted for both ED2 and ED2-BL to investigate the mechanisms driving changes in spatial heterogeneity. Each set of ensemble runs kept all model parameters constant except for the soil texture. Thirty different soil textures, defined through the set of pedotransfer functions described above, were used. Specifically, the soil texture data from 15 RAINFOR sites were used plus an additional 15 sites selected to cover the full range of soil texture triangle (*Fig. S4, Table S5*).

These simulations were initialized with a near-bare-ground ecosystem state and run to equilibrium under 2005 atmospheric CO_2 levels (378ppm). A constant CO_2 value was used to remove any transient CO_2 fertilization effects.

Four meteorological drivers were used to force the ensemble runs; a driver with a two-month DSL, a four-month DSL, a six-month DSL, and an eight-month DSL. The four drivers were created using tower meteorological data from the RAINFOR site Manaus KM34 (30) and precipitation from the downscaled Sheffield dataset (5) in order to create the desired dry season length. Specific humidity and shortwave radiation were adjusted using the observed relationship between precipitation, temperature, specific humidity, and shortwave radiation in the tower observations. The result was four internally consistent drivers that were identical except for their DSL, and corresponding changes in specific humidity and shortwave radiation. A two month interval between drivers was chosen because a two month increase in dry season length, or 100 mm decrease in maximum climatological water deficit (defined as in *Malhi et al*. (31)), is similar to the projected change for the Amazon basin over the 21st century (31). The results of these simulations are shown in *Figure 2 (main text).*

A second set of ensemble runs was conducted in which water stress (both γ_{WS}, defined in the main text, and drought-deciduous phenology) was eliminated. In these runs (ED2-NWS), plant growth rates were not influenced by soil moisture (i.e. γ_{WS} =0 in Eq.*(1)*). The results of these simulations are shown in *Figure S5.*

Finally, the impact of changes in dry season length was investigated using the 30 soil texture ensemble runs and a suite of different climate scenarios. The equilibrium forests spun-up under 2-month, 4-month, and 6-month dry seasons were subjected to a one to four month increase in dry season length. The drivers were created in the same way as described above such

that they were internally consistent. These simulations were conducted for 200 years. The results of these simulations are shown in *Figure 3 (main text)*.

Table S3a: Life history, physiological, and allometric parameters of different plant functional types used in ED2 and ED2-BL

Property	**Early-successional**	**Mid-successional**	**Late-successional**
V_{m0} (μmol m^{-2} s^{-1})*	18.75	12.50	6.25
Leaf lifespan (year)	1	2	3
Wood Density (g cm^{-3})	0.53	0.71	0.90
Specific leaf area (m^2 kgC^{-1})	16	11.6	9.7
Density independent mortality (μ_{PFT_i}, yr^{-1})	0.0617	0.0317	0.0

* Consistent with other 'big-leaf' ecosystem models formulations (*e.g. Collatz et al. (32)* which is the basis for the photosynthetic formulation for most terrestrial ecosystem models), the V_{m0} values in ED2-BL were increased to 75 for early-successional tropical trees, 50 for mid-successional tropical trees, and 25 for late-successional tropical trees. This increase is necessary to compensate for the loss of vertical structure in the ED2-BL canopy. For further discussion of this issue, see *Moorcroft et al.* (22).

Allometric relationships for Leaf and Wood Biomass (kg C) as a function of tree diameter (DBH, in cm):

$$Leaf\ biomass = {}^{a}/_{2} * DBH^{b}$$
$$Wood\ biomass = {}^{c}/_{2} * DBH^{d} \qquad (DBH \leq DBH_{\max})$$
$$Wood\ biomass = {}^{e}/_{2} * DBH^{f} \qquad (DBH > DBH_{max})$$

Table S3b: Allometric parameters for the tropical forest tree PFTs. Note that the coefficients for wood biomass reflect the influence of wood density on the woody biomass allometry function.

Property	**Early-successional**		**Mid-successional**		**Late-successional**	
	ED2	ED2-BL	ED2	ED2-BL	ED2	ED2-BL
a	0.0591	0.0732	0.0695	0.0758	0.0791	0.0892
b	1.5706	1.509	1.5634	1.647	1.5577	1.663
c	0.159	0.159	0.214	0.214	0.271	0.269
d	2.441	2.343	2.441	2.371	2.441	2.254
e	0.1748	0.159	0.234	0.214	0.297	0.269
f	2.422	2.343	2.422	2.371	2.422	2.254

Table S4: RAINFOR sites used to evaluate the predictions of the ED2 biosphere model.

Plot Name	Plot Code	Lat	Lon	Soil Depth (m)	Soil Type	Sand Fraction (xsand)	Clay Fraction (xclay)
Santarém KM 67	S67	-2.86	-54.96	8m	Clay	0.02	0.9
Reserva Pé-de-Gigante	PDG	-21.62	-47.65	6m	Loamy sand	0.85	0.03
Manaus	M34	-2.61	-60.21	8m	Clay	0.2	0.68
Reserva Biológica Jarú	RJA	-10.08	-61.93	2m	Loamy sand	0.8	0.1
Tambopata	TAM	-12.83	-69.27	2m	Clay	0.4	0.43
Caxiuanã	CAX-06	-1.72	-51.46	4m	Clay	0.38	0.44
Caxiuanã	CAX-08	-1.86	-51.44	4m	Clay Loam	0.40	0.39
Allpahuayo	ALP	-3.95	-73.44	4m	Sand	0.937	0.026
La Lorena	LOR	-3.06	-69.99	1.25m	Clay Loam	0.38	0.31

Table S5: Clay, sand and silt fractions for the 30 sites that were used for the ensemble runs.

Site name	**Soil Type**	**Sand Fraction** (xsand)	**Clay fraction** (xclay)
S67	Clay	0.02	0.90
S77	Clay	0.18	0.80
M34	Clay	0.20	0.68
TNF	Clay	0.38	0.60
--	Clay	0.20	0.60
CAX-06	Clay	0.38	0.44
TAM-05	Clay	0.40	0.43
CAX-08	Clayey loam	0.40	0.39
BAN	Clayey loam	0.24	0.37
--	Clayey loam	0.32	0.34
LOR-01	Clayey loam	0.38	0.31
--	Clayey sand	0.375	0.525
--	Clayey silt	0.125	0.525
--	Heavy clay	0.10	0.80
--	Loam	0.41	0.17
KEN	Loamy sand	0.76	0.16
RJA	Loamy sand	0.80	0.10
-	Loamy sand	0.825	0.06
PDG	Loamy sand	0.85	0.03
ZAR-01	Loamy sand	0.748	0.006
--	Sand	0.92	0.03
ALP-21	Sand	0.937	0.026
--	Sandy clay	0.52	0.42
--	Sandy clay loam	0.59	0.27
CAX	Sandy loam	0.78	0.15
--	Sandy loam	0.66	0.11
--	Silt	0.075	0.05
--	Silty clay	0.06	0.47
--	Silty clay loam	0.10	0.34
--	Silty loam	0.20	0.16

SI Appendix S4: Comparison Between ED2 Model Simulations and Observations

Regional comparison: A good relationship is observed between AGB from regional ED2 simulations conducted with a basin wide soil map and both the *Saatchi et al*. (2) and *Baccini et al*. (1) remote-sensing based estimates (*Fig. 1 main text, Fig. S6*). In addition, the spatial pattern of AGB across the basin produced by the ED2 regional simulation is consistent with the remote-sensing based estimates of *Baccini et al*. (1) and *Saatchi et al*. (2) (*Fig. S7* (13)), with the ED2 model reproducing the observed continuous distribution of AGB across the basin from high biomass forest to low biomass savannah (*Fig. 1b main text*). The ED2 model simulations also replicate the observed trend of higher spatial variability in AGB with longer dry season length for the forested sites (AGB > 2 kg C m^{-2}), with increasing site-to-site AGB variability (1σ/mean) from 3.6% for a 1-2 month DSL to 37.4% for a 5-6 month dry season (*Fig. 1c main text*). This is in contrast to the ED2-BL simulations that result in a significantly different spatial pattern of AGB with a bi-modal distribution of biomass (*Fig. 1b main text*, *and Fig. S7*), a pattern similar to those seen in other 'big-leaf' models when run without fire (e.g. 13).

The ED2 model also captures the basin-wide observed trends of AGB variability in relation to soil texture and dry season length, with generally good agreement between both the mean and variability of modeled AGB and remote-sensing based estimates across the observed range of soil clay fractions and dry seasons (*Fig. S8*). The model does underestimate the observed variability in AGB when dry season length is short, potentially due to the impact of spatial variation in soil fertility that is not represented in the model simulations and has been shown to influence AGB on both local (17, 21) and basin (15, 16) scales. The average modeled AGB for dry season lengths greater than 6 months is lower than remote sensing based estimates; however, the range in predicted values is consistent with the observations. In addition to model

error, uncertainty and biases in the climatological forcing and inaccuracies in the soil map and variations in soil texture with depth will contribute to the observed mismatches.

Site-level comparison: The difference between high biomass moist tropical forests and drier more transitional forests involves more than simply a change in above-ground biomass (AGB). Differences in AGB across the Amazon basin have been shown to correlate with stem turnover rate (33) and mean wood density (34): high biomass forests have lower stem turnover rates and higher mean wood densities. Mean wood density has previously been used as an axis for characterizing forest composition (16, 20, 22, 34), reflecting results from empirical studies that tropical tree species with lower wood densities tend to have higher growth and mortality rates than higher wood density species (e.g. 16, 20, 22, 34). The size-structure of the forest also varies with AGB, with high biomass forests characterized by a higher ratio of biomass in large trees relative to small trees (*Fig. S9b*). Here we evaluate the ability for ED2 to capture these fundamental underlying dynamics of the regions forests.

While there are some disagreements between the predicted and observed magnitudes, the model correctly reproduces the observed negative correlation between AGB and stem turnover rate (15, 33), the shift in the distribution of AGB across size-classes with increasing total biomass, and the positive correlation between AGB and wood density (20, 34, 36) (*Fig. S9*). Here we quantify the size-structure of the forest as the structural asymmetry (γ_{sa}) of the basal areas versus diameter (DBH) size class distribution of the forest canopy (37). γ_{sa} provides a measure of the amount of basal area in large trees relative to small trees and is defined as the skewness of the best-fit lognormal distribution to the tree diameter data (*Fig. S10*):

$$\gamma_{sa} = \sqrt{e^{\sigma^2} - 1\left(2 + e^{\sigma^2}\right)}$$

where σ is the standard deviation of the lognormal distribution. γ_{sa} was calculated for RAINFOR network plots (38) using data curated by ForestPlots.net (35, 39, 40). The observational plot data used in the model-observational comparison (*Fig. S9 and S11*) are provided in *SI Appendix Tables S1*, *S6*, and *S7*.

The difference in the predicted and observed magnitude of the emergent stand-level relationships between wood density and AGB seen in Fig. S9c may be due to the representation of a small number of plant functional types (PFTs) within the model. In ED2, the 'late-successional' tree PFT has a wood density of 0.9, a value significantly higher than the wood densities observed in the RAINFOR plots where the majority (±1σ) of individuals have a wood density between 0.3 and 0.8, and only 0-2% have a wood density of 0.9 or higher. Better agreement is seen if the observations are instead grouped by functional type. For example, at Manaus KM34, the model simulation results in a canopy with an average community composition of 53% mid-successional trees, which is consistent with the observed value of 55% (where mid-successional trees are defined as individuals with wood densities between 0.6 and 0.8).

With regard to canopy dynamics, ED2 accurately captures the timing and magnitude of the diurnal cycle of flux-tower based estimates of gross primary production (*Fig. S11a*) and the observed rate of change in above-ground biomass (*Fig. S11b*). In addition, the modeled relationship between mortality and biomass is qualitatively consistent with the observations, although the mortality rates in ED2 are elevated with respect to the observations (*Fig. S9a*). An analysis of South and Central American stem mortality data from Condit *et al*. (41) shows that the density independent mortality rates used in ED2 fall within the observed range for all three topical tree functional types. Observed mortality rates for the late successional plant functional

type (1.5%, range 0.4-5.3%) are consistent with the value used in ED2 (1.4%) and the underlying relationship between density independent mortality and wood density (Fig 9c) is qualitatively correct but too strong in magnitude (22, 41, 42). It is also important to recognize that plot based observations of mortality rates are subject to sampling biases which will tend to underestimate the frequency of infrequent large scale disturbance events and so underestimate background mortality rates (43). Further work is needed to fully investigate the variability of density independent mortality rates within functional groups in order to better constrain this relationship.

Table S6: RAINFOR data used for model-observation comparison. Data are calculated from stem-level census data, which can be found at ForestPlots.net, using the equation for structural asymmetry (SI 4) and the allometric relationship of Baker et al. (34). The mean value for the observational period is used.

Site Name	Plot	Years	AGB	Structural Skewness
ALP	11	1990-2009	13.52	1.60
ALP	12	1990-2009	13.43	1.78
ALP	21	1990-2009	11.81	1.58
ALP	22	1990-2009	12.00	1.49
ALP	30	2001-2009	10.94	1.62
ALP	40	2006-2009	10.87	1.06
CAX	01	1994-2004	17.66	1.81
CAX	02	1995-2003	17.17	1.80
LOR	01	2004-2006	12.06	1.49
LOR	02	1992-2006	14.17	1.72
LOR	03	1992-2006	14.37	1.65
PDG		2003	2.87	0.94
TAM	01	1979-2008	11.17	1.50
TAM	02	1983-2008	12.66	1.45
TAM	05	1983-2008	12.39	1.65
TAM	06	1983-2008	12.19	1.57
TAM	07	1983-2008	12.66	1.58
TAM	08	1983-2008	10.24	1.50

Site Name	Plot	Years	AGB	Structural Skewness
PDBFF	1101_1	1981-2003	15.50	1.71
PDBFF	1102_1	1981-2003	13.77	1.63
PDBFF	1103_1	1981-2003	13.74	1.58
PDBFF	1105_1	1981-2003	16.42	1.67
PDBFF	1109_1	1981-2003	15.28	1.70
PDBFF	1113_1	1987-2002	17.55	1.75
PDBFF	1201_1	1281-2003	14.94	1.54
PDBFF	1201_2	1281-2003	16.22	1.70
PDBFF	1201_3	1281-2003	11.15	1.41
PDBFF	1301_1	1983-2002	15.49	1.61
PDBFF	1301_4	1983-2002	17.82	1.80
PDBFF	1301_5	1983-2002	16.13	1.63
PDBFF	1301_6	1983-2002	17.33	1.68
PDBFF	1301_7	1983-2002	17.43	1.61
PDBFF	1301_8	1983-2002	19.77	1.83
PDBFF	2303_5	1985-2002	17.46	1.62
PDBFF	2303_6	1985-2002	16.87	1.55
PDBFF	3304_8	1984-2003	18.83	1.67
PDBFF	3304_9	1984-2003	18.49	1.66
PDBFF	3401_1	1985-2003	16.59	1.72
PDBFF	3402_2	1985-2003	16.65	1.76
PDBFF	3402_3	1985-2003	15.03	1.54
PDBFF	3402_4	1985-2003	17.32	1.80
PDBFF	3402_5	1985-2003	15.74	1.69
PDBFF	3402_6	1985-2003	16.70	1.79
PDBFF	3402_7	1985-2003	15.32	1.59
PDBFF	3402_8	1985-2003	13.87	1.65
PDBFF	3402_9	1985-2003	16.81	1.74

Table S7: Annual mean diurnal cycle of gross primary production for the Manaus K34 (2002-2005) and Santarem KM67 (2002-2004) sites based on flux tower data analyzed by Restrepo-Coupe et al (2013).

Hour	Mean Hourly GPP (kg m^{-2} yr^{-1})	
	M34	S67
0	0	0
1	0	0
2	0	0
3	0	0
4	0	0
5	0	0
6	0	0
7	0	0
8	0	0
9	0	0
10	0	0.22
11	2.28	5.54
12	4.89	7.90
13	7.83	8.86
14	9.97	9.31
15	10.71	9.00
16	10.63	8.44
17	10.01	7.38
18	8.85	6.04
19	7.20	4.50
20	5.28	2.51
21	3.05	0.49
22	0.57	0.00
23	0.02	0.00

SI Appendix S5: ED2 Model Response to Variation in Water-stress and Soil Texture

For ED2, all soil-texture ensemble runs with a 2- to 6-month dry season showed a gradual transition from high biomass forests to low biomass forests, with an average decrease in AGB of 22.5% (range: -12.9% to -64.4%) for a two month decrease in dry-season from a 4- to a 6-month dry season (*Fig. 2 main text*). In contrast to the ED2 runs, but similar to the ED2-BL regional simulation, ED2-BL ensemble runs resulted in two stable ecosystems with a 6-month dry season resulting in either a high biomass (*N=29*) forest, with an average decrease in AGB of 3.9% (range: -0.3% to -15.2%) relative to the 4 month dry season simulations, or a low biomass savannah (*N=1*) with a 98.6% decrease in AGB relative to the 4-month dry season simulations (*Fig. 2 main text*). This two state outcome is even more apparent in the ED2-BL simulations with 8-month dry season.

For a given meteorological driver, the average plant water stress (γ_{WS} main text equation 1) in the forested sites increased with increasing soil clay content in the ED2 model simulations (*Fig. 2a main text*) (r^2=0.74-0.82 p<0.01). This reflects the high water retention of the clay matrix that decreases the amount of water available for plant uptake; however, as can be seen in the figure, the relationship between plant water stress and soil clay content varies as a function of dry season length. When AGB values are plotted as a function of average plant water stress (γ_{WS}), the differing relationships between AGB and soil clay content seen in *Figure 2a* collapse onto a single line, with AGB declining strongly and monotonically as a function of average plant water stress in a manner that is independent dry season length (r^2=0.96-0.99, p<0.01) (*Fig. 2c main text*). The corresponding relationships for ED2-BL model simulations are shown in *Figures 2b* and *2d*. As can be seen in *Figure 2d*, at low values of water stress (γ_{WS}), the ED2-BL ensemble simulations show a similar but less pronounced decline in AGB in response to increasing γ_{WS}

(*Fig. 2d*); however, once γ_{WS} exceeds ~0.15-0.2, a tipping point is reached after which AGB declines markedly as high biomass forests are replaced by low biomass savannah ecosystems. This indicates that the response of individual plants to water availability plays an important role in determining AGB particularly in transitional forests.

To confirm the role of water stress in governing AGB in the ED2 model simulations, an additional set of model ensemble simulations were conducted in which plant growth rates are not influenced by soil moisture (ED2-NWS). When water stress is excluded from the model simulations, the variability of the equilibrium AGB for the soil ensemble simulations drops below 2% (*Fig. S5*); specifically, from 1.7% to 0.3% (DSL = 2 months), from 3.4% to 0.6% (DSL = 4 months), 19.9% to 1.7% (DSL = 6 months), and from 11.6% to 0.9% (DSL = 8 months). Differences between the four ED2-NWS model simulations derive from differences in canopy specific humidity, canopy temperature, and incoming short-wave radiation that accompany the reduction precipitation.

SI Appendix S6: Individual-scale dynamics of water-stress in ED2

ED2 represents individual-scale dynamics within a horizontally and vertically heterogeneous plant canopy (*see SI Appendix S3 for a detailed description of the model*). The impacts of this heterogeneity are illustrated in *Figure S12* which shows, for two soils with differing clay contents, how individual-level plant water stress varies as a function of both plant size and functional type, and the resulting net mean canopy level water stress. In both soils, levels of water stress vary between individuals as function of their size and plant functional type (*Figure S12*). These differences in water stress between individuals reflect underlying differences in the allometric properties of individuals (e.g. taller trees have deeper roots than small trees), and differences in the underlying biochemical, physiological, and biomechanical traits of the PFTs (*Table S3a*). In the case depicted in *Figure S12*, individuals of the mid-successional PFT generally experiencing higher plant levels of water stress than those of the late-successional PFT. In addition, levels of plant water stress are generally higher in the soil with higher clay content (panel b) compared to soil with low clay content (panel a); however, the difference varies by individual as a function of both the plant size and plant functional type. The resulting mean canopy-level water stress is determined by the distribution of individual-level water stress values weighted by the abundance (density) of plants of different sizes and types. As illustrated in the figure (dashed horizontal lines in panels a and b), the mean canopy water stress differs substantially from those predicted by the aggregated ED2-BL model.

Associated with the changes in above-ground biomass that occur in the ED2 model ensemble runs with varying soil texture (*SI Appendix S5*), are associated changes in the ecosystem function and composition. By way of illustration, *Figure S13* shows how, for a forest with a six-month dry season, changes in soil texture alter patterns of net primary productivity

(NPP), and plant functional type composition of the plant canopy. As soil clay fraction increases, levels of water stress in both the upper and mid-canopy increase. However, as can be seen in panels a and c, the net primary productivity (NPP) of upper canopy trees (50-70cm) declines at lower levels of water stress than the NPP of mid-canopy trees (10-30cm). This effect is due to the combined impact of water stress and light levels on NPP: as water stress increases, the canopy becomes more open, and, as a result, the remaining canopy and mid-story trees experience higher levels of incoming light availability (indicated by the colors of the points in panels a and c). As can be seen in panels *b* and *d* of the figure, the higher levels of light availability, in addition to influencing NPP, also cause the canopy composition to shift away from shade-tolerant trees towards higher abundance of more light-adapted mid-successional trees (*Fig. S13c and d*).

SI Appendix S7: Above-Ground Biomass Sensitivity to Changes in Dry Season Length

A suite of model simulations was conducted to test the impact of a 1-4 month change in dry season length on forest AGB. Currently ~11% of the Amazon basin experiences a dry season of 2-3 months, 20% experiences a dry season of 3-4 months, ~24% experiences a dry season of 4-5 months, ~16% experiences a dry season of 5-6 months, and ~10% experiences a dry season of greater than 6 months (*Table S8*). Our results suggest that, for a significant portion of the Amazon, AGB may decrease by ~20% with a 2 month increase in dry season length.

An increase in dry season length (DSL) results in increased mortality and decreased growth within the first few years following the perturbation (*Fig. S14 and Fig. S15*). A subsequent shift in community composition is seen as the forest re-assembles, shifting away from late-successional shade-tolerant species to mid-successional species (*Fig. 3 main text and Fig. S14*). A concurrent shift in forest structure is seen as high mortality in the large size class trees immediately following the perturbation results in a canopy with a higher proportion of small trees (*Fig. S15*).

Table S8: Impact of change in dry season on forest biomass after 100 years.

AGB change kg C m^{-2} $century^{-1}$	**1 month increase in DSL**	**2 month increase in DSL**	**3 month increase in DSL**	**4 month increase in DSL**
Forest with 2 month DSL	-0.18 ± 0.08 (min -0.06, max -0.31)	-0.58 ± 0.26 (min -0.13, max -1.41)	-1.81 ± 1.16 (min -0.69, max -6.27)	-2.90 ± 1.41 (min -1.89, max -7.85)
Forest with 4 month DSL	-1.21 ± 0.94 (min -0.50, max -4.87)	-2.89 ± 1.48 (min -1.77, max -7.48)	-5.84 ± 0.93 (min -4.37, max -8.69)	-11.49 ± 1.02 (min -9.14, max -13.04)
Forest with 6 month DSL	-3.42 ± 0.83 (min -1.34, max -5.08)	-8.26 ± 2.12 (min -2.61, max -10.32)		

AGB % change	**1 month increase in DSL**	**2 month increase in DSL**	**3 month increase in DSL**	**4 month increase in DSL**
Forest with 2 month DSL	-1.13% ± 0.49% (min -0.37%, max -2.00%)	-3.62% ± 1.71% (min -0.79%, max -9.22%)	-11.51% ± 7.98% (min -4.19%, max -42.46%)	-18.44% ± 9.85% (min - 11.64%, max - 53.66%)
Forest with 4 month DSL	-8.24% ± 7.21% (min -3.15%, max -37.29%)	-19.49% ± 11.67% (min -11.24%, max -58.03%)	-38.70% ± 8.17% (min -28.53%, max -67.67%)	-79.21% ±- 2.73% (min -72.78%, max -83.34%)
Forest with 6 month DSL	-28.69% ± 3.72% (min -19.59%, max -37.49%)	-72.47% ± 6.64% (min -56.75%, max -80.60%)		

References:

1. Baccini A*, et al.* (2012) Estimated carbon dioxide emissions from tropical deforestation improved by carbon-density maps. *Nature Climate Change* 2(3):182-185.

2. Saatchi SS*, et al.* (2011) Benchmark map of forest carbon stocks in tropical regions across three continents. *Proceedings of the National Academy of Sciences of the United States of America* 108(24):9899-9904.

3. Baker TR*, et al.* (2004) Increasing biomass in Amazonian forest plots. *Philosophical Transactions of the Royal Society of London Series B-Biological Sciences* 359(1443):353-365.

4. Arino O, Ramos J, Kalogirou V, Defourny P, & Achard F eds (2010) *GlobCover 2009,* Bergen, Norway.

5. Sheffield J, Goteti G, & Wood EF (2006) Development of a 50-year high-resolution global dataset of meteorological forcings for land surface modeling. *Journal of Climate* 19(13):3088-3111.

6. INPE (2013) Monitoramento da Floresta Amazônica Brasileira por Satélite (São José dos Campos, Brazil).

7. Nepstad D*, et al.* (2004) Amazon drought and its implications for forest flammability and tree growth: a basin-wide analysis. *Global Change Biology* 10(5):704-717.

8. Rocha W*, et al.* (2013) Ecosystem productivity and carbon cycling in intact and annually burnt forest at the dry southern limit of the Amazon rainforest (Mato Grosso, Brazil). *Plant Ecology & Diversity*.

9. Balch JK, Massad TJ, Brando PM, Nepstad DC, & Curran LM (2013) Effects of high-frequency understorey fires on woody plant regeneration in southeastern Amazonian forests. *Philosophical Transactions of the Royal Society B-Biological Sciences* 368(1619).

10. Brando PM*, et al.* (2014) Abrupt increases in Amazonian tree mortality due to drought–fire interactions. *Proceedings of the National Academy of Sciences* 111(17):6347-6352.

11. Nepstad DC, Tohver IM, Ray D, Moutinho P, & Cardinot G (2007) Mortality of large trees and lianas following experimental drought in an amazon forest. *Ecology* 88(9):2259-2269.

12. Nepstad DC, *et al.* (2002) The effects of partial throughfall exclusion on canopy processes, aboveground production, and biogeochemistry of an Amazon forest. *Journal of Geophysical Research-Atmospheres* 107(D20).

13. Zhang K, *et al.* (2015) The Fate of Amazonian Ecosystems over the Coming Century Arising from Changes in Climate, Amospheric CO_2 and Land Use. *Global Change Biology* 21(7):2569–2587. doi: 10.1111/gcb.12903.

14. Malhi Y, *et al.* (2004) The above-ground coarse wood productivity of 104 Neotropical forest plots. *Global Change Biology* 10(5):563-591.

15. Quesada CA, *et al.* (2012) Basin-wide variations in Amazon forest structure and function are mediated by both soils and climate. *Biogeosciences* 9(6):2203-2246.

16. ter Steege H, *et al.* (2006) Continental-scale patterns of canopy tree composition and function across Amazonia. *Nature* 443(7110):444-447.

17. Laurance WF, *et al.* (1999) Relationship between soils and Amazon forest biomass: a landscape-scale study. *Forest Ecology and Management* 118(1–3):127-138.

18. Quesada CA, *et al.* (2010) Variations in chemical and physical properties of Amazon forest soils in relation to their genesis. *Biogeosciences* 7(5):1515-1541.

19. IGBP-DIS, Global Soil Task 2000, Global Soil Data Products CD_ROM (http://www.daac.ornl.gov/SOILS/igbp.html).

20. Baraloto C, *et al.* (2011) Disentangling stand and environmental correlates of aboveground biomass in Amazonian forests. *Global Change Biology* 17(8):2677-2688.

21. Jimenez EM, *et al.* (2014) Edaphic controls on ecosystem-level carbon allocation in two contrasting Amazon forests. *Journal of Geophysical Research-Biogeosciences* 119(9):1820-1830.

22. Moorcroft PR, Hurtt GC, & Pacala SW (2001) A method for scaling vegetation dynamics: The ecosystem demography model (ED). *Ecological Monographs* 71(4):557-585.

23. Medvigy D, Wofsy SC, Munger JW, Hollinger DY, & Moorcroft PR (2009) Mechanistic scaling of ecosystem function and dynamics in space and time: Ecosystem Demography model version 2. *Journal of Geophysical Research-Biogeosciences* 114.

24. Cosby BJ, Hornberger GM, Clapp RB, & Ginn TR (1984) A statistical exploration of the relationships of soil-moisture characteristics to the physical-properties of soil. *Water Resources Research* 20(6):682-690.

25. Clapp RB & Hornberger GM (1978) Empirical equations for some soil hydraulic-properties. *Water Resources Research* 14(4):601-604.

26. Foley JA*, et al.* (1996) An integrated biosphere model of land surface processes, terrestrial carbon balance, and vegetation dynamics. *Global Biogeochemical Cycles* 10(4):603-628.

27. Levis S, Bonan GB, Vertenstein M, & Oleson KW (2004) The Community Land Model's Dynamic Global Vegetation Model (CLM-DGVM): Technical description and user's guide. in *NCAR Technical Note NCAR/TN-459+IA* (National Center for Atmospheric Research, Boulder, CO).

28. Goudriaan J (1977) *Crop Micrometeorology: A Simulation Study* (Cent. for Agric. Publ. Doc., Wageningen, Netherlands).

29. Nakicenovic N*, et al.* (2000) IPCC Special report on emissions scenarios. (Cambridge, UK & New York, NY, USA), p 599.

30. Restrepo-Coupe N*, et al.* (2013) What drives the seasonality of photosynthesis across the Amazon basin? A cross-site analysis of eddy flux tower measurements from the Brasil flux network. *Agricultural and Forest Meteorology* 182–183:128-144.

31. Malhi Y*, et al.* (2009) Exploring the likelihood and mechanism of a climate-change-induced dieback of the Amazon rainforest. *Proceedings of the National Academy of Sciences* 106(49):20610-20615.

32. Collatz GJ, Ball JT, Grivet C, & Berry JA (1991) Physiological and environmental regulation of stomatal conductance, photosynthesis and transpiration: a model that includes a laminar boundary layer. *Agricultural and Forest Meteorology* 54(2-4):107-136.

33. Phillips OL*, et al.* (2004) Pattern and process in Amazon tree turnover, 1976-2001. *Philosophical Transactions of the Royal Society of London Series B-Biological Sciences* 359(1443):381-407.

34. Baker TR*, et al.* (2004) Variation in wood density determines spatial patterns in Amazonian forest biomass. *Global Change Biology* 10(5):545-562.

35. Lopez-Gonzalez G, Lewis SL, Burkitt M, & Phillips OL (2011) ForestPlots.net: a web application and research tool to manage and analyse tropical forest plot data. *Journal of Vegetation Science* 22(4):610-613.

36. Galbraith D*, et al.* (2013) Residence times of woody biomass in tropical forests. *Plant Ecology & Diversity* 6(1):139-157.

37. Wright SJ, Muller-Landau HC, Condit R, & Hubbell SP (2003) Gap-dependent recruitment, realized vital rates, and size distributions of tropical trees. *Ecology* 84(12):3174-3185.

38. Malhi Y*, et al.* (2002) An international network to monitor the structure, composition and dynamics of Amazonian forests (RAINFOR). *Journal of Vegetation Science* 13(3):439-450.

39. Lopez-Gonzalez G, Lewis SL, Phillips OL, Burkitt M, & Baker TR, ForestPlots.net Database. http://www.forestplots.net. Date of extraction 21/10/2010.

40. Lopez-Gonzalez G, Burkitt M, Lewis SL, & Phillips OL (2012) ForestPlots.net – managing permanent plot information across the tropics. *Vegetation databases for the 21st century, -- Biodiversity & Ecology* 4:95-103.

41. Condit R*, et al.* (2006) The importance of demographic niches to tree diversity. *Science* 313(5783):98-101.

42. Longo M (2014) Amazon forest response to changes in rainfall regime: results from an individual-based dynamic vegetation model. PhD (Harvard University).

43. Chambers JQ*, et al.* (2013) The steady-state mosaic of disturbance and succession across an old-growth Central Amazon forest landscape. *Proceedings of the National Academy of Sciences of the United States of America* 110(10):3949-3954.

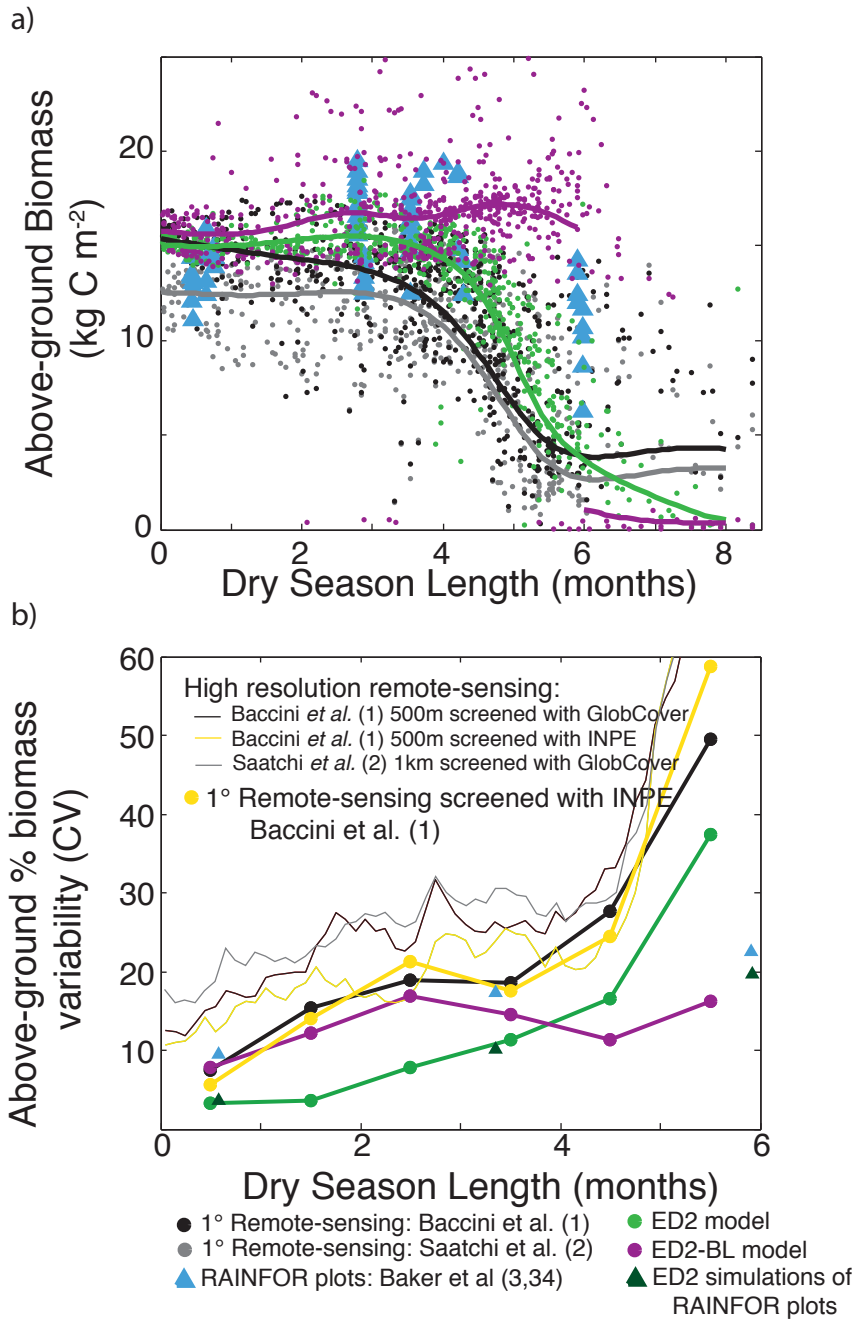

Figure S1: a) change in above-ground biomass with dry season length for remote-sensing based estimates (black and gray circles), ground-based plot measurements (blue triangles), ED2 model output (green circles), and ED2-BL model output (purple circles). Tendlines for each of the regional dataset are added using a cubic smoothing spline. A break is seen in the trend line for the ED2-BL model because no data is present between AGB=11.28 and AGB=0.99. b) displays the coefficient of variation (σ/μ) using GlobCover and INPE data to generate the remote-sensing primary vegetation datasets. The coefficients of variation for the RAINFOR plots (blue triangles) and ED2 simulations of RAINFOR plots (green triangles) are also shown.

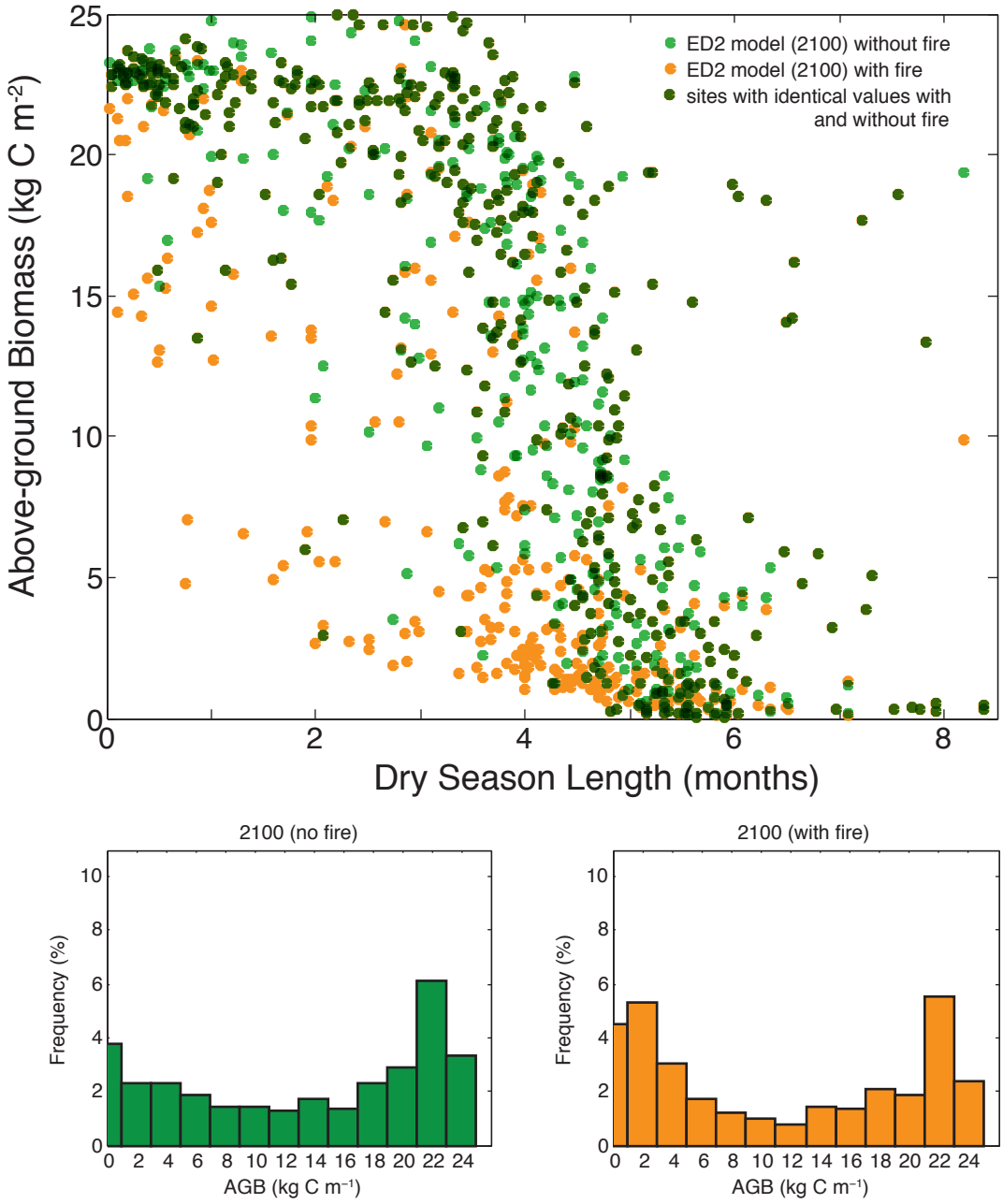

Figure S2: Change in above-ground biomass (AGB) with dry season length and the distribution of AGB across the basin for regional ED2 simulations with-out (green) and with (orange) fire from Zhang *et al.* (13). Model projections for 2100 are shown.

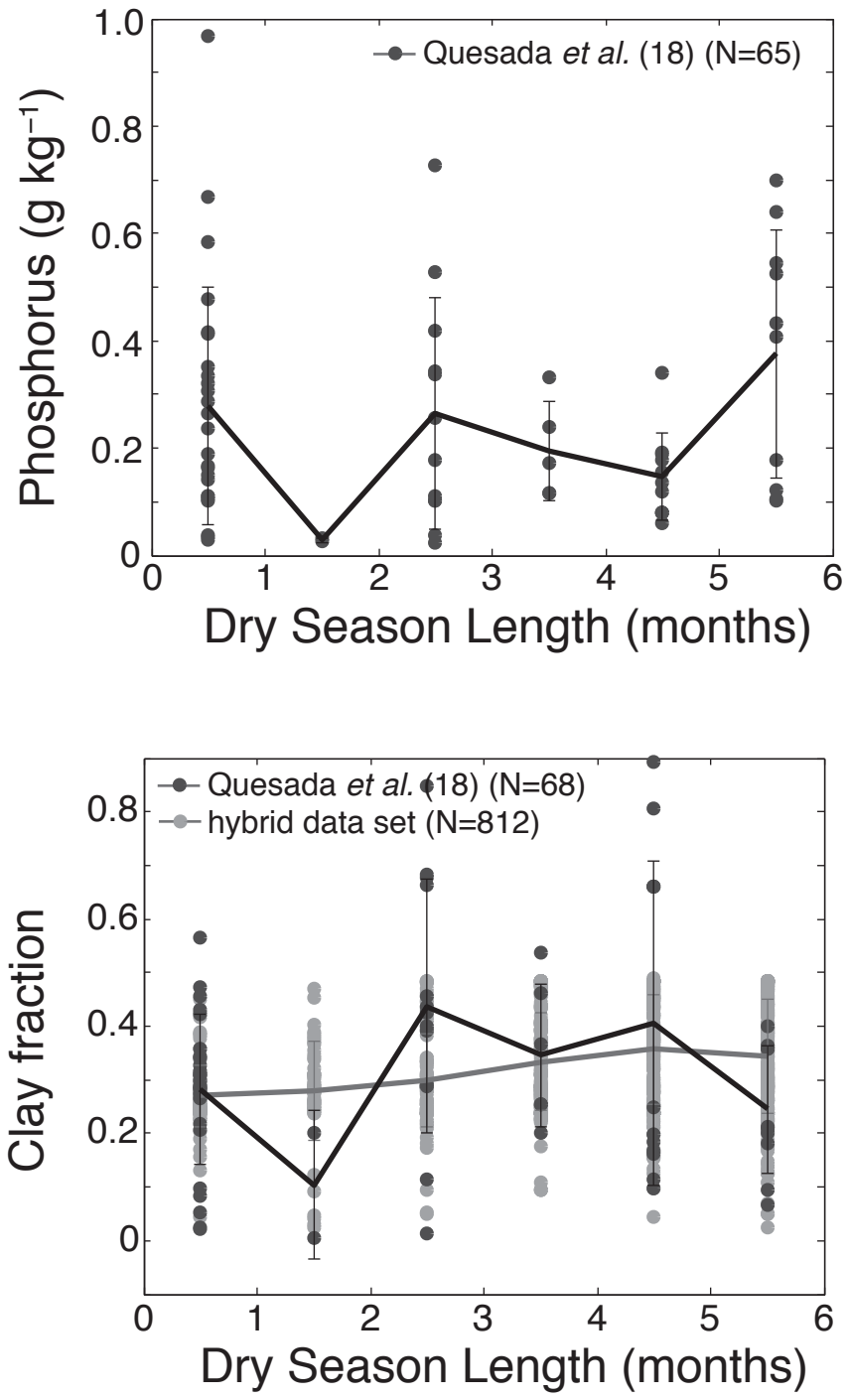

Figure S3: Change in soil phosphorus content (proxy for fertility) and soil clay fraction (proxy for soil texture) with change in dry season length (DSL). The number of data points (N) for each dataset is given. No significant relationship is obseved between phosphorus or clay content and DSL in the Quesada *et al.* (18) dataset. A slight increase in clay fraction with increasing DSL is seen in the hybrid dataset.

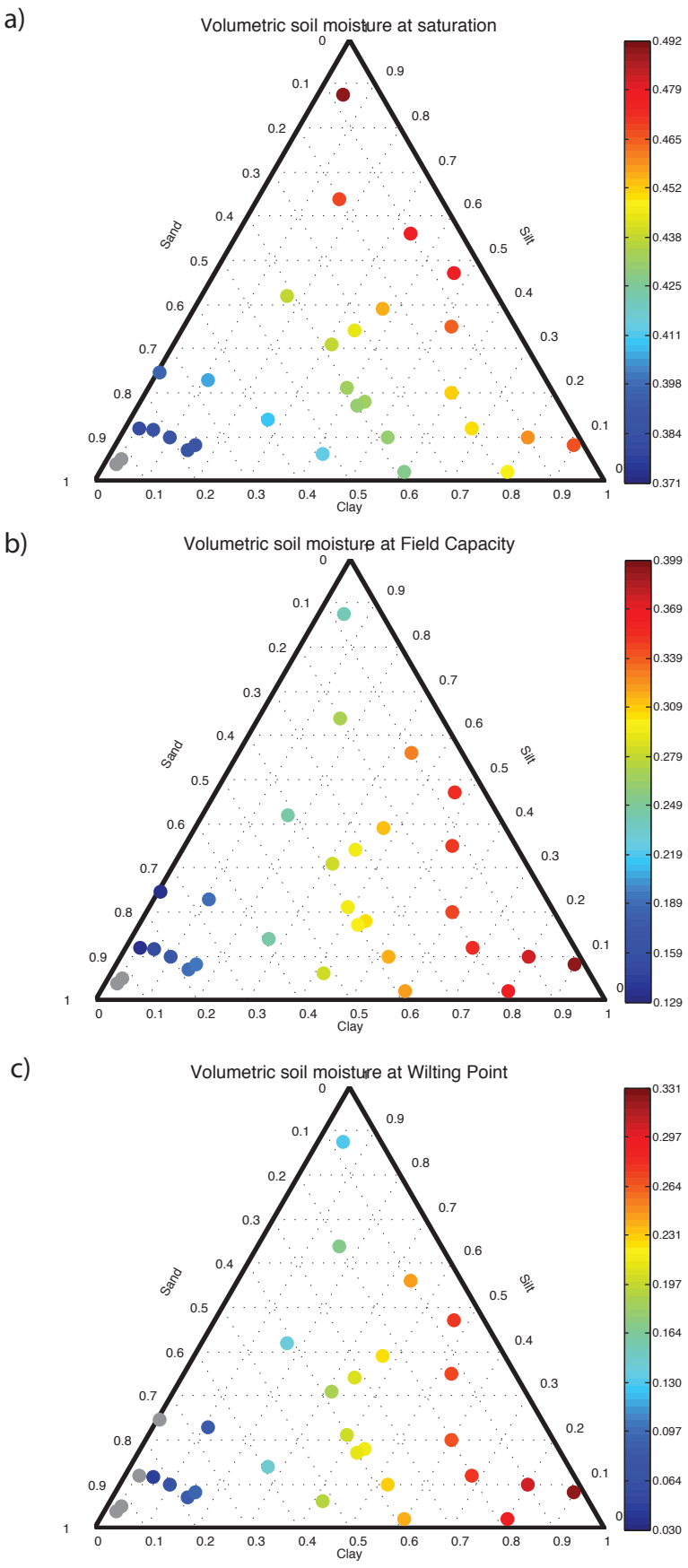

Figure S4: Soil properties for the 30 soil types used for the ensemble model runs.

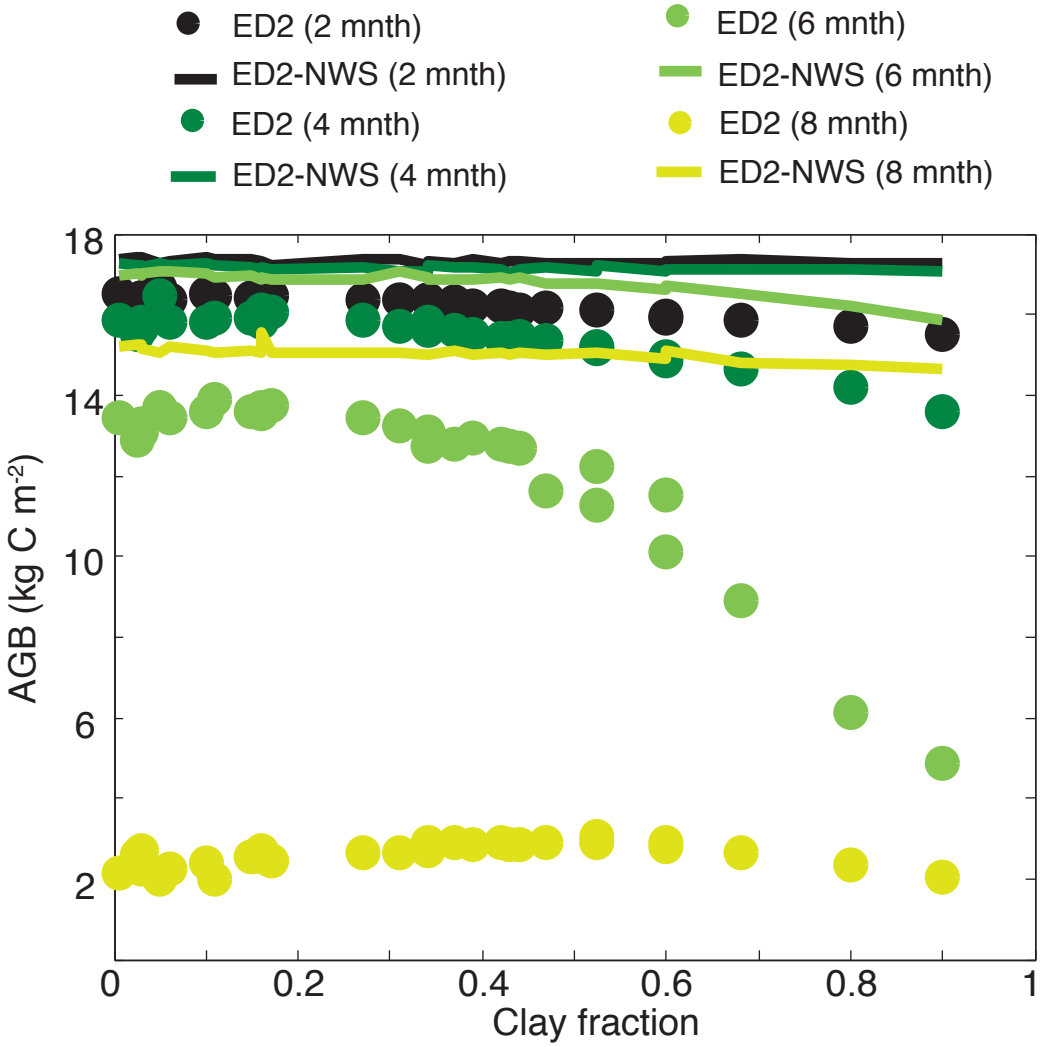

Figure S5: Impact of changes in soil clay fraction on above-ground biomass (AGB) in ED2 (circles) and in ED2 in the absence of water stress (ED2-NWS, lines). Four climatological conditions are shown, a 2-month dry season, a 4-month dry season, a 6-month dry season and an 8-month dry season.

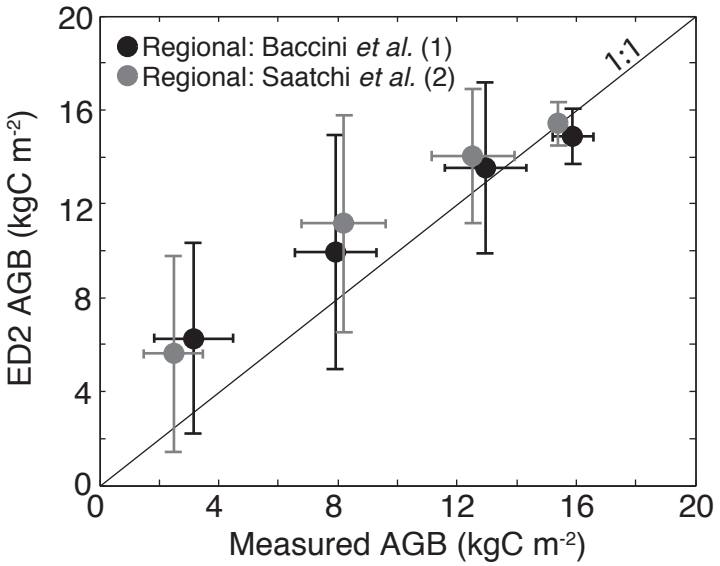

Figure S6: The relationship between predicted and remote-sensing based estimates of AGB for regional simulations of the Amazon basin. The data are binned by AGB (0-5, 5-10, 10-15, 15-20) and the error bars denote variability within a bin for regional data.

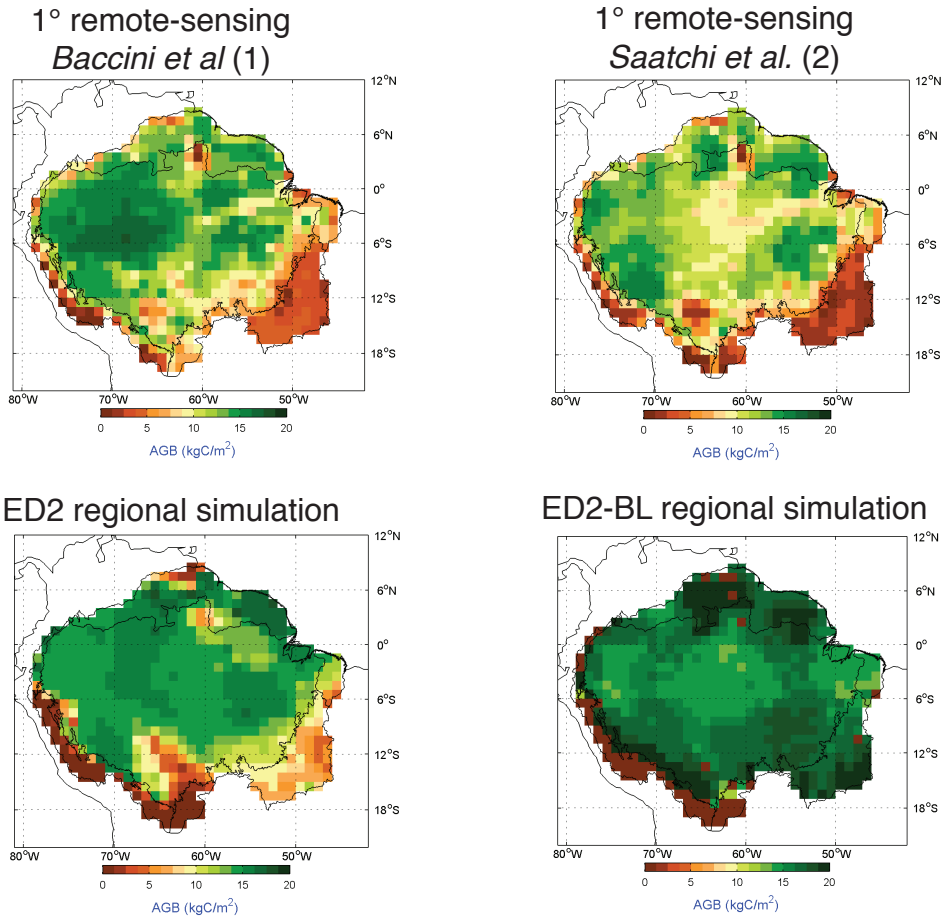

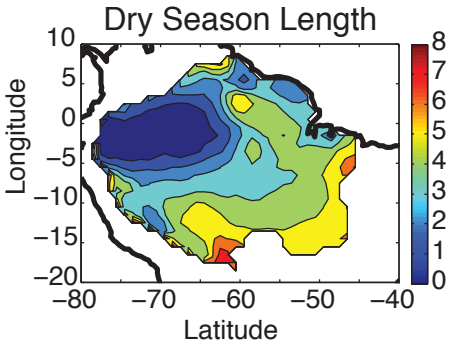

Figure S7: Regional maps of above-ground biomass from remote-sensing estimates (*1,2*) and model output (ED2 and ED2-BL). Remote-sensing estimates are aggregated to 1° for comparison to the model output. Note that the model does not simulate river dynamics and so does not capture the low biomass region on the banks of the Amazon river. A map of dry season length based on the *Sheffield et al.* (5) climatology is also shown.

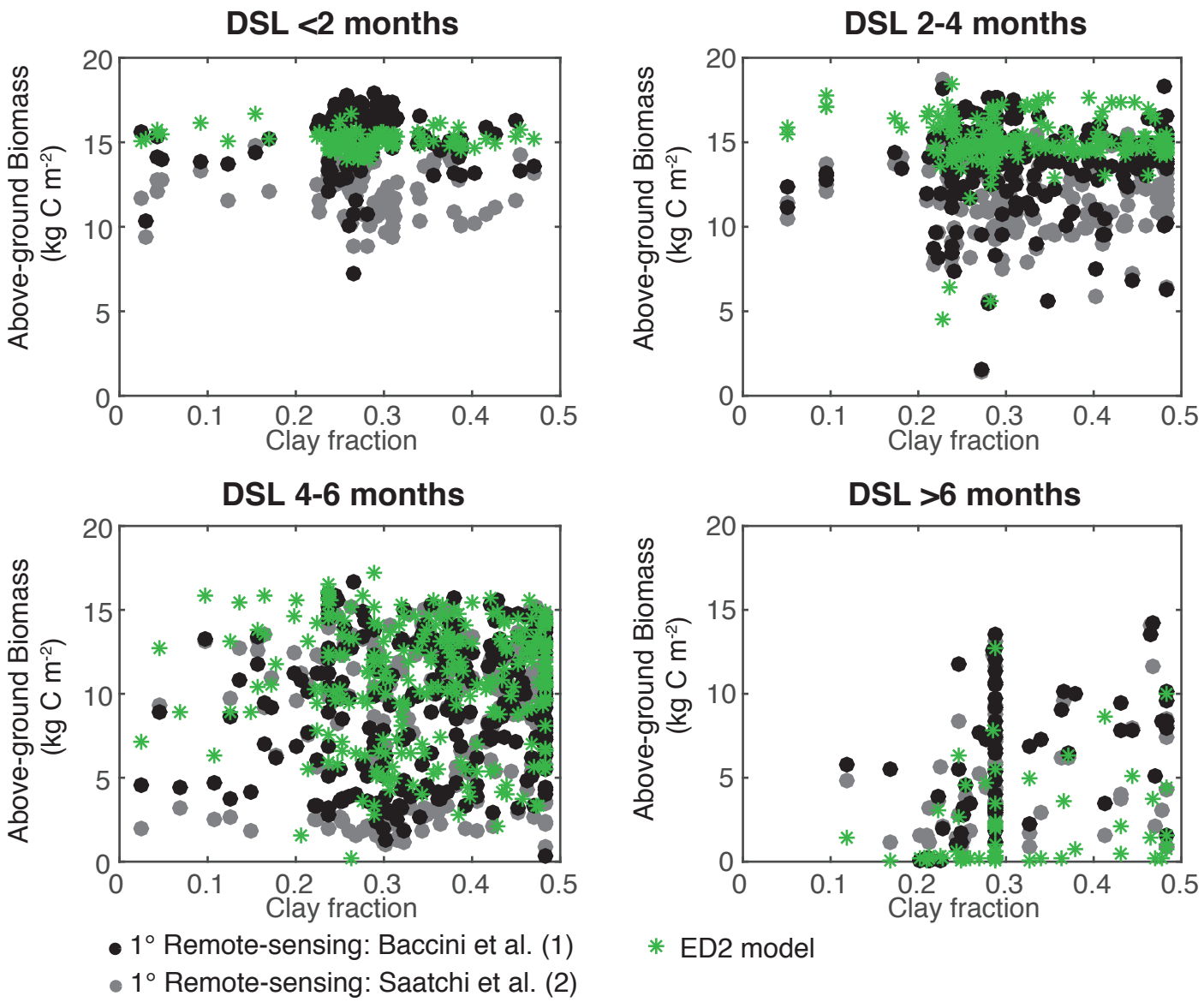

Figure S8: Comparison between regional ED2 model predictions (green) and remote-sensing based estimates (black and gray) of basin-wide spatial variation in above-ground biomass (AGB) plotted as a function of dry season length (DSL) and soil clay fraction.

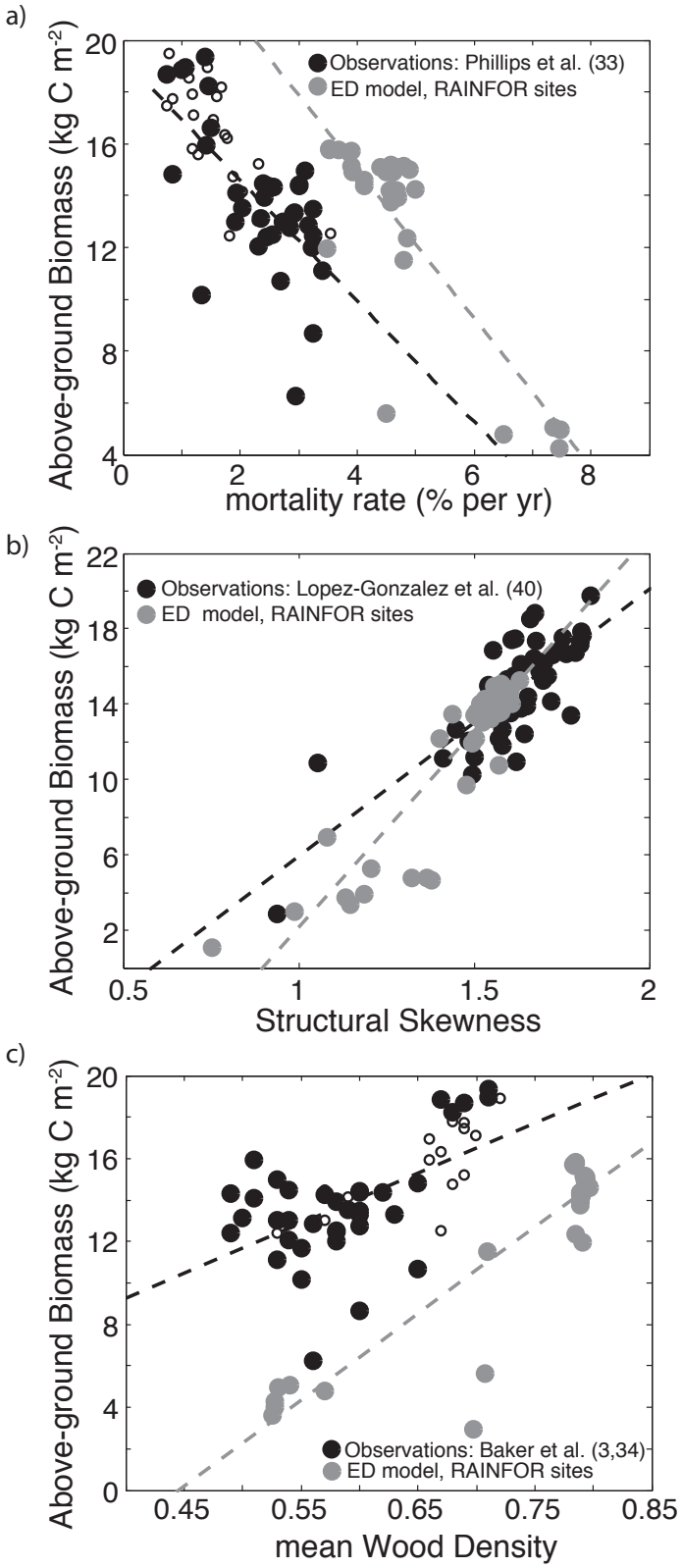

Figure S9: Variation in forest function (a), structure (b), and composition (c) with above-ground biomass for plot based observations (3, 33, 34, 40) (black) and ED2 model output for select RAINFOR sites (grey). Filled black circles denote observations for which corresponding model simulations were conducted. Open circles denote observations without a corresponding model simulation.

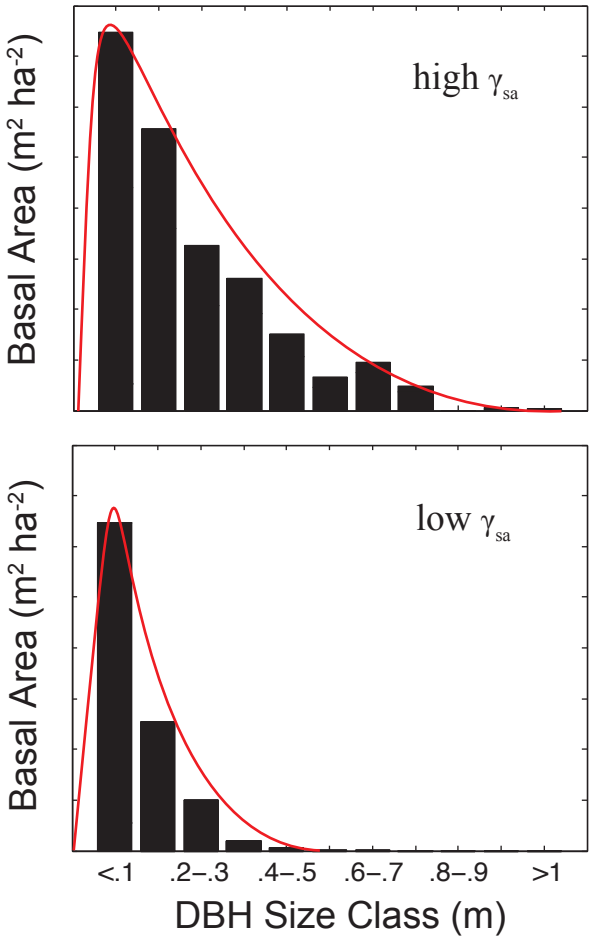

Figure S10: Example of the calculation of structural asymmetry (γ_{sa}). γ_{sa} is defined as the skewness of the best-fit lognormal distribution (red line) to tree diameter data (black bars). γ_{sa} is a measure of canopy structure by quantifying the relative amount of small to large trees.

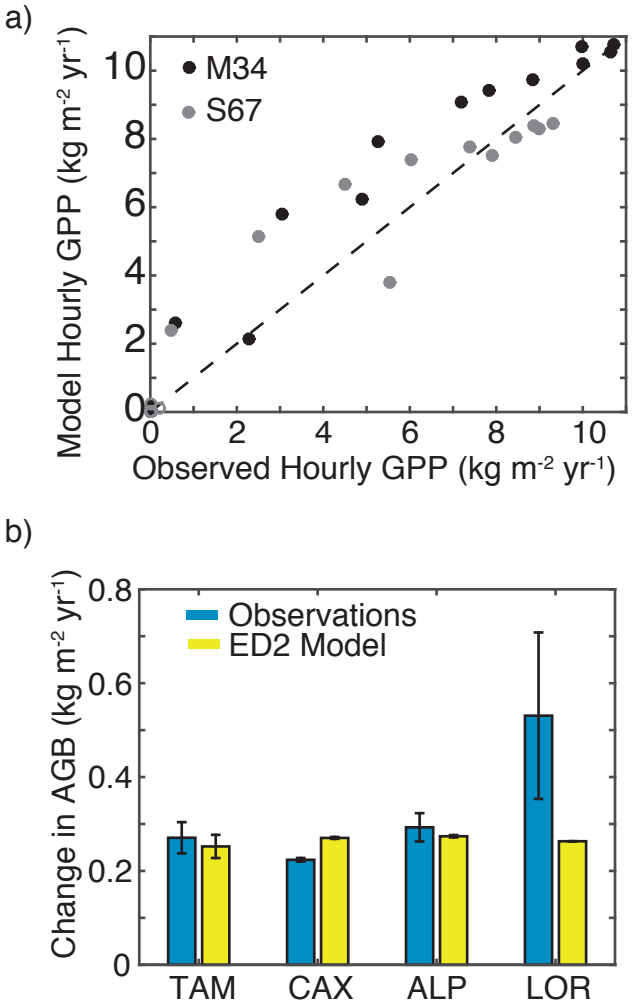

Figure S11: Panel a) relationship between the observed and modeled mean diurnal cycle of gross primary production (GPP), calculated as hourly averages for flux-tower based estimates and ED2 model output at Manaus KM34 (2002-2005) and Santarem KM67 (2002-2004). Panel b) average annual change in AGB for TAM, CAX, ALP, and LOR for plot based estimates (blue) and ED2 model output (yellow).

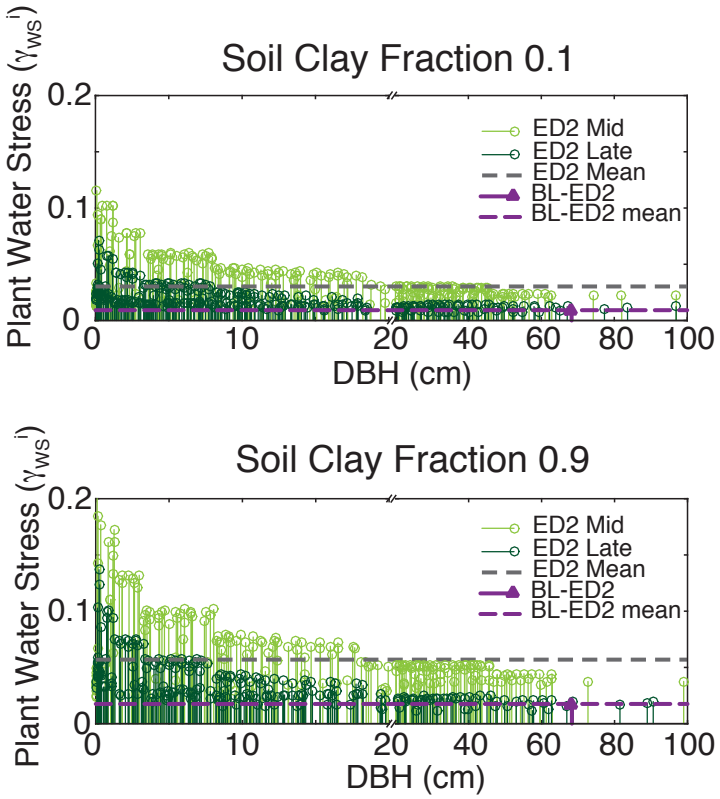

Figure S12: Vertical lines show the individual-level plant water stress (γ_{WS}^{i}) by size (DBH) and colored according to their functional type (PFT, mid-successional and late-successional). Model output for a dry season length of 4 months and two soil types (soil clay fraction = 0.1 and 0.9) are shown. The variation in plant water stress (γ_{WS}^{i}) for a given DBH and PFT reflects horizontal heterogeneity in moisture availability arising from canopy-gap dynamics within ED2. The resulting mean canopy-scale water stress (grey dashed line) is also shown. The canopy-scale water stress in the corresponding ED2-BL simulations are also shown (purple dashed line). Note the break in scale at 20 cm DBH.

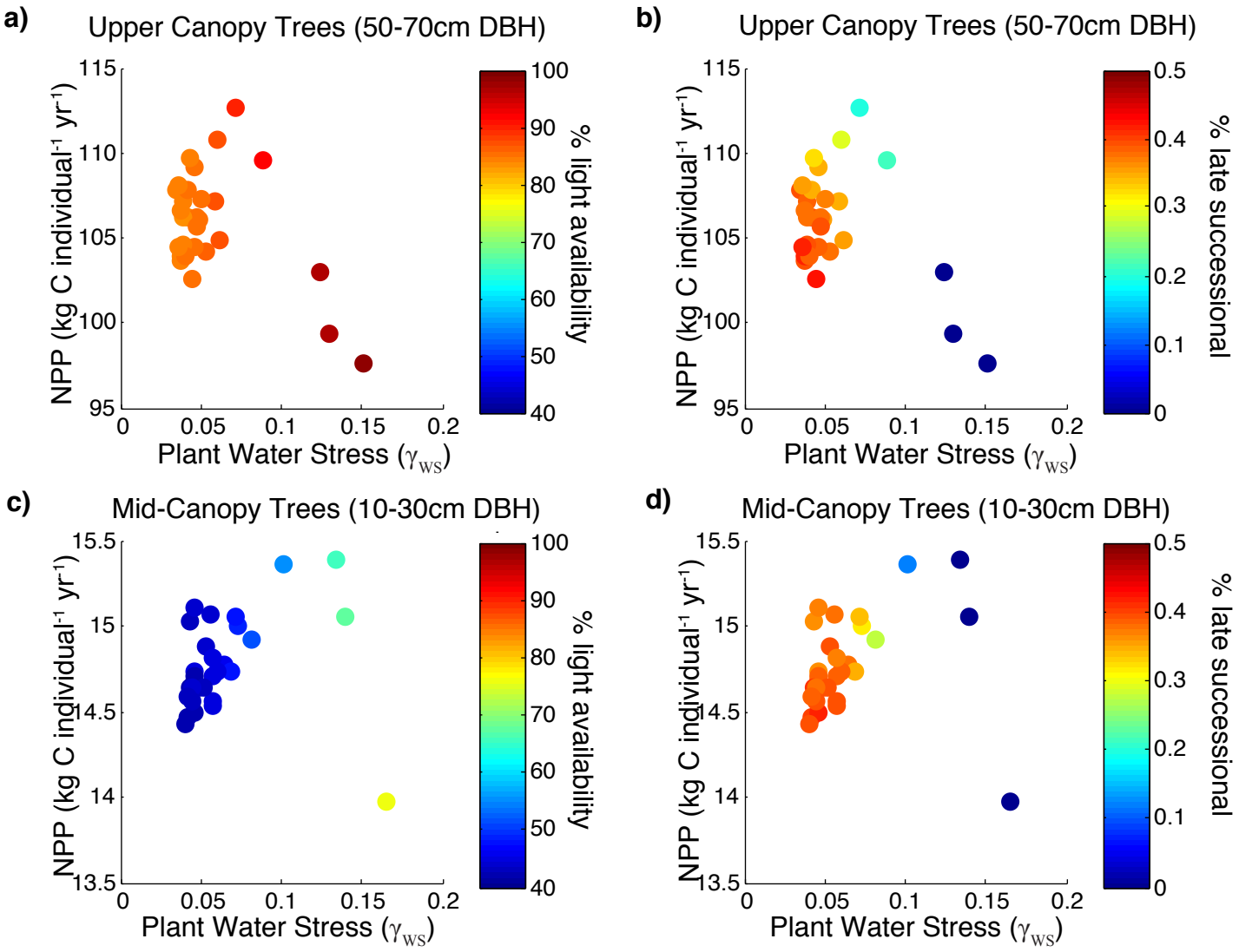

Figure S13: The impacts of changes in soil texture on ecosystem function and composition for a forest canopy with a six-month dry season. The points in each panel indicate the outcome of simulations for a range of 30 soil types shown in Figure S4. The relationship between net primary productivity of individual's (NPP) and water stress is shown for upper canopy trees (50-70cm DBH, panels a and b) and mid-canopy trees (10-30cm DBH, panels c and d). The colors in panels a and c indicate the mean light level of individuals in the specified size class. The mean composition of the upper and mid-canopy trees is shown by the symbol color in panels b and d, respectively. Panels a and c illustrate how increasing levels of water stress associated with increasing soil clay content causes changes in NPP in the upper canopy (panel a) and mid-canopy (panel c). The NPP of upper canopy trees declines once their water stress (γ_{WS}) increases above 0.08 (panel a), while mid-canopy trees do not experience the negative effect of water stress until their water stress level (γ_{WS}) exceeds 0.14 (panel c). As indicated by the colors of the points in panels a and c, the differential impact of water stress on the upper and mid-canopy is linked to correlated changes in light availability: as water stress increases, light levels in both the upper and lower canopy increase due to the increased rates of mortality in the plant canopy. Panels b and d illustrate the correlated shifts in plant canopy composition that are associated with the changes in levels of plant water stress and net primary productivity as soil texture changes. As levels of water stress increase and levels of light availability in the canopy increase, the abundance of late-successional trees declines as indicted by the colors of the points in panels b and d.

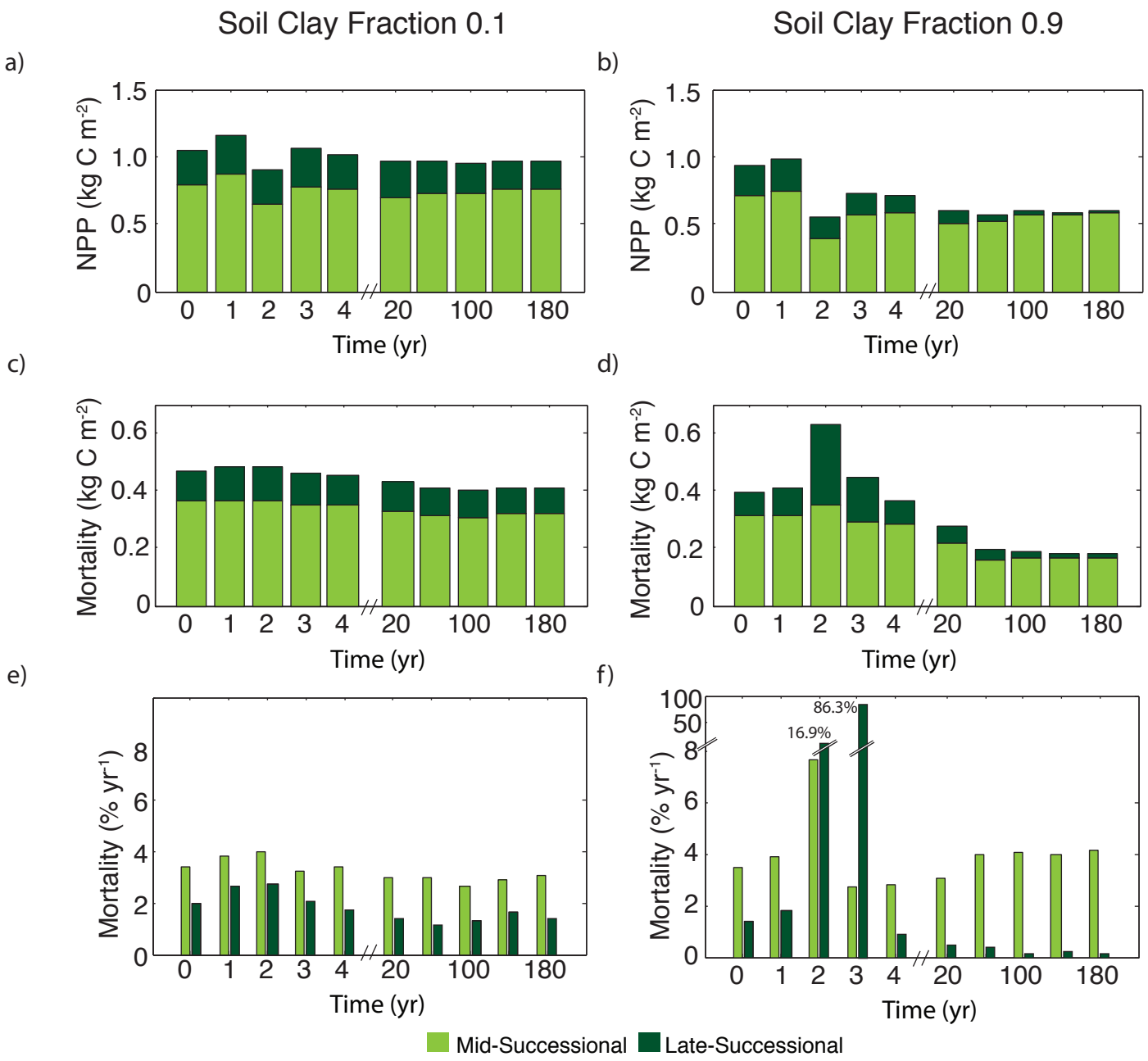

Figure S14: Predicted changes in forest growth and mortality in response to a 2-month increase in dry season length (from 4 to 6 months) on two different soil types. Panels (a) and (b) show the predicted changes in net primary production (NPP), and panels (c) and (d) show the changes in mortality than underpin the changes in above-ground biomass dynamics shown in Fig.3. Panels e) and f) show the same results as in panels c) and d) but expressed as percent mortality per year. The color of the bars indicates the contribution of mid- and late- successional trees to the stand-level growth and mortality. At the low soil clay fraction site (panels a and c), the changes in rates of growth and mortality are relatively small. In contrast, at the site with a high soil clay fraction (panels b and d), NPP decreases and mortality increases significantly in the first few years after a drought is imposed, particularly for late-successional trees.

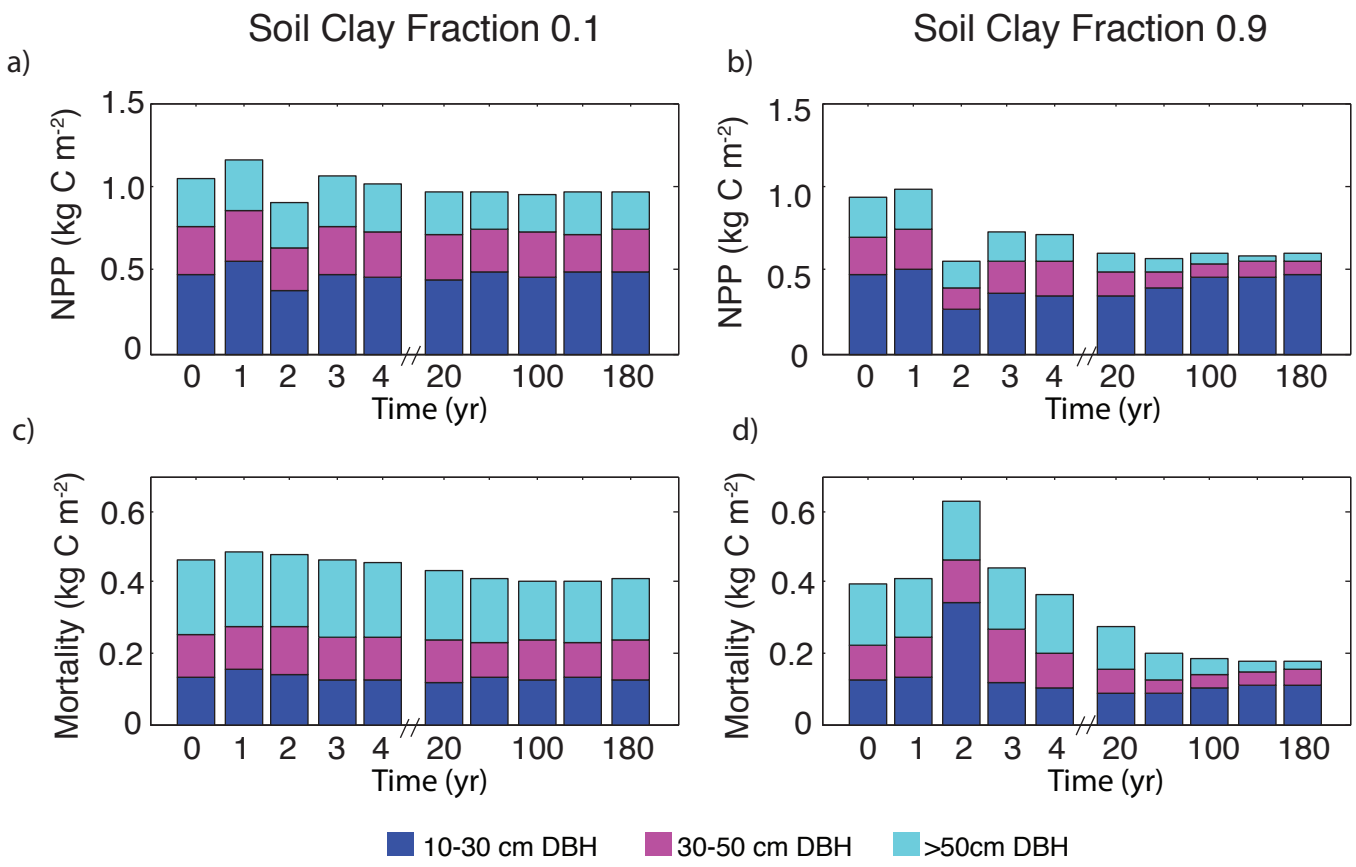

Figure S15: Predicted changes in forest growth and mortality in response to a 2-month increase in dry season length (from 4 to 6 months) on two different soil types. Panels (a) and (b) show the predicted changes in net primary production (NPP), and panels (c) and (d) show the change in mortality than underpin the changes in above-ground biomass dynamics shown in Fig.3. The color of the bars indicates the contribution of different tree diameter (DBH) size classes: 10-30cm DBH, 30-50cm DBH, and greater than 50cm DBH. At the low soil clay fraction site (panels a and c), the changes in rates of growth and mortality are relatively small. In contrast, at the high clay fraction site (panels b and d), NPP decreases and mortality increases in response to increasing DSL, and the contribution of large trees to overall NPP and mortality declines.